ICDT 2016

The Eleventh International Conference on Digital Telecommunications

ISBN: 978-1-61208-454-1

February 21 - 25, 2016

Lisbon, Portugal

ICDT 2016 Editors

Marko Jäntti, University of Eastern Finland, Finland
Sathiamoorthy Manoharan, University of Auckland, New Zealand

ICDT 2016

Forward

The Eleventh International Conference on Digital Telecommunications (ICDT 2016), held between February 21-25, 2016 in Lisbon, Portugal, continued a series of events focusing on telecommunications aspects in multimedia environments. The scope of the conference was to focus on the lower layers of systems interaction and identify the technical challenges and the most recent achievements.

High quality software is not an accident; it is constructed via a systematic plan that demands familiarity with analytical techniques, architectural design methodologies, implementation polices, and testing techniques. Software architecture plays an important role in the development of today's complex software systems. Furthermore, our ability to model and reason about the architectural properties of a system built from existing components is of great concern to modern system developers.

Performance, scalability and suitability to specific domains raise the challenging efforts for gathering special requirements, capture temporal constraints, and implement service-oriented requirements. The complexity of the systems requires an early stage adoption of advanced paradigms for adaptive and self-adaptive features.

Online monitoring applications, in which continuous queries operate in near real-time over rapid and unbounded "streams" of data such as telephone call records, sensor readings, web usage logs, network packet traces, are fundamentally different from traditional data management. The difference is induced by the fact that in applications such as network monitoring, telecommunications data management, manufacturing, sensor networks, and others, data takes the form of continuous data streams rather than finite stored data sets. As a result, clients require long-running continuous queries as opposed to one-time queries. These requirements lead to reconsider data management and processing of complex and numerous continuous queries over data streams, as current database systems and data processing methods are not suitable.

The conference had the following tracks:

- Digital communications

We take here the opportunity to warmly thank all the members of the ICDT 2016 technical program committee, as well as all the reviewers. The creation of such a high quality conference program would not have been possible without their involvement. We also kindly thank all the authors that dedicated much of their time and effort to contribute to ICDT 2016. We truly believe that, thanks to all these efforts, the final conference program consisted of top quality contributions.

Also, this event could not have been a reality without the support of many individuals, organizations and sponsors. We also gratefully thank the members of the ICDT 2016 organizing

committee for their help in handling the logistics and for their work that made this professional meeting a success.

We hope ICDT 2016 was a successful international forum for the exchange of ideas and results between academia and industry and to promote further progress in the areas of telecommunications in multimedia environments. We also hope that Lisbon, Portugal provided a pleasant environment during the conference and everyone saved some time to enjoy the beauty of the city.

ICDT 2016 Advisory Committee

Constantin Paleologu, University Politehnica of Bucharest, Romania
Tomohiko Taniguchi, Fujitsu Laboratories Limited, Japan
Jaime Lloret Mauri, Polytechnic University of Valencia, Spain
Abdulrahman Yarali, Murray State University, USA
Michael Grottke, University of Erlangen-Nuremberg, Germany
Javier Del Ser Lorente, TECNALIA RESEARCH & INNOVATION - Zamudio, Spain
Saied Abedi, Fujitsu Laboratories of Europe Ltd. (FLE), UK
Gerard Damm, Alcatel-Lucent, USA
Dan Romascanu, Avaya, Israel
Klaus Drechsler, Fraunhofer Institute for Computer Graphics Research IGD - Darmstadt, Germany

ICDT 2016

Committee

ICDT 2016 Advisory Committee

Constantin Paleologu, University Politehnica of Bucharest, Romania
Tomohiko Taniguchi, Fujitsu Laboratories Limited, Japan
Jaime Lloret Mauri, Polytechnic University of Valencia, Spain
Abdulrahman Yarali, Murray State University, USA
Michael Grottke, University of Erlangen-Nuremberg, Germany
Javier Del Ser Lorente, TECNALIA RESEARCH & INNOVATION - Zamudio, Spain
Saied Abedi, Fujitsu Laboratories of Europe Ltd. (FLE), UK
Gerard Damm, Alcatel-Lucent, USA
Dan Romascanu, Avaya, Israel
Klaus Drechsler, Fraunhofer Institute for Computer Graphics Research IGD - Darmstadt, Germany

ICDT 2016 Technical Program Committee

Antonio Marcos Alberti, INATEL - Instituto Nacional de Telecomunicações, Brazil
Abdullah M. Alnajim, Qassim University, Saudi Arabia
Maria Teresa Andrade, FEUP / INESC Porto, Portugal
Iosif Androulidakis, MPS Jozef Stefan, Slovenia
Regina B. Araujo, Federal University of São Carlos, Brazil
Khaled Assaleh, American University of Sharjah, United Arab Emirates
Anteneh Ayanso, Brock University, Canada
Francisco Barcelo-Arroyo, Technical University of Catalonia, Spain
Ilija Basicevic, University of Novi Sad, Serbia
Carlos Becker Westphall, Federal University of Santa Catarina, Brazil
Abdelouahab Bentrcia, King Saud University – Riyadh, Kingdom of Saudi Arabia
Massudi bin Mahmuddin, University Utara Malaysia, Malaysia
Andrzej Borys, Gdynia Maritime University - Gdynia, Poland
Damian Bulira, Wroclaw University of Technology, Poland
Ladislav Burita, University of Defence in Brno / Tomas Bata University in Zlin, Czech Republic
Andi Buzo, University Politehnica of Bucharest, Romania
Lee-Ming Cheng, City University of Hong Kong, Hong Kong
Alberto Coen-Porisini, Università degli Studi dell'Insubria – Varese, Italy
Doru Constantin, University of Pitesti, Romania
Gerard Damm, Alcatel-Lucent, USA
Klaus Drechsler, Fraunhofer-Institut für Graphische Datenverarbeitung IGD - Darmstadt,

Copyright Information

For your reference, this is the text governing the copyright release for material published by IARIA.

The copyright release is a transfer of publication rights, which allows IARIA and its partners to drive the dissemination of the published material. This allows IARIA to give articles increased visibility via distribution, inclusion in libraries, and arrangements for submission to indexes.

I, the undersigned, declare that the article is original, and that I represent the authors of this article in the copyright release matters. If this work has been done as work-for-hire, I have obtained all necessary clearances to execute a copyright release. I hereby irrevocably transfer exclusive copyright for this material to IARIA. I give IARIA permission or reproduce the work in any media format such as, but not limited to, print, digital, or electronic. I give IARIA permission to distribute the materials without restriction to any institutions or individuals. I give IARIA permission to submit the work for inclusion in article repositories as IARIA sees fit.

I, the undersigned, declare that to the best of my knowledge, the article is does not contain libelous or otherwise unlawful contents or invading the right of privacy or infringing on a proprietary right.

Following the copyright release, any circulated version of the article must bear the copyright notice and any header and footer information that IARIA applies to the published article.

IARIA grants royalty-free permission to the authors to disseminate the work, under the above provisions, for any academic, commercial, or industrial use. IARIA grants royalty-free permission to any individuals or institutions to make the article available electronically, online, or in print.

IARIA acknowledges that rights to any algorithm, process, procedure, apparatus, or articles of manufacture remain with the authors and their employers.

I, the undersigned, understand that IARIA will not be liable, in contract, tort (including, without limitation, negligence), pre-contract or other representations (other than fraudulent misrepresentations) or otherwise in connection with the publication of my work.

Exception to the above is made for work-for-hire performed while employed by the government. In that case, copyright to the material remains with the said government. The rightful owners (authors and government entity) grant unlimited and unrestricted permission to IARIA, IARIA's contractors, and IARIA's partners to further distribute the work.

Table of Contents

Tracking Sound Source Localization for a Home Robot Application

Gil Lopes, Andreia Albernaz, Hélder Ribeiro, Fernando Ribeiro
Algoritmi Research Center
Dpt. Industrial Electronics, University of Minho
Guimaraes, Portugal
e-mail: gil@dei.uminho.pt
andreialbernaz13@gmail.com
a58795@alunos.uminho.pt
fernando@dei.uminho.pt

M. S. Martins
CMEMS, University of Minho
Campus of Azurém, Guimarães, Portugal
LARSyS, University of Algarve
Campus de Gambelas, PT-8005-139 Faro, Portugal
e-mail: mmartins@dei.uminho.pt

***Abstract*—The future of robotics is now trending for home servicing. Nursing homes and assistance to elder people are areas where robots can provide valuable help in order to improve the quality of life of those who need it most. Calling a robot, for a person of age, can be a daunting task if the voice is failing and any resort to battery operated devices fails to comply. Using a simple mechanical apparatus, such as a Click trainer for dogs, a person can call a robot by pressing the button of a powerless device. The high pitch sound produced by this device can be captured and tracked down in order to estimate the person's location within a room. This paper describes a method that provides good accuracy and uses simple and low cost technology, in order to provide an efficient positional value for an assistance robot to attend its caller. The robot does not need to search for the person in a room as it can directly travel towards the Click's sound source.**

Keywords-localization; sound source; interaural sound difference; time difference of arrival

I. INTRODUCTION

The use of home robots is in demand specially in tasks such as dust cleaning and food cooking. The future is promising and an increase of research is being held in areas of robotic assistance in industry, hospitals and also at home. In the latter case, the Robocup@Home competition [1] is contributing with valuable research and development of robotic solutions for home assistance with demanding tasks that increase in difficulty and complexity every year.

One of the main targets for home assistance is the help for elderly people, where normal daily activities could be improved if a personal assistant was always present. This is the case of nursing homes, where usually this task is taken care of by the regular staff. They are in charge of responding to calls of elder people when any type of assistance is necessary (to get hold of some object such as a book, TV remote, food, beverages, etc.). An assistance robot can be the helping hand 24/7.

In that sense, calling a robot can be performed in different ways. The first approach is vocal and therefore it is still a viable solution for calling someone or a machine if the person's voice is healthy. That is not the case generally for elder people. A second approach is via electronic means, such as battery operated remote controller or a button on a wall. Electronic devices need energy to operate and both present weaknesses. Batteries on a remote controller can run or dim out and the assistance cannot be called. This builds up stress on the caller that keeps pressing the button without any response from the assistant. A button on the wall does not rely on batteries to operate but on the ability of the caller to walk to it. For an elder person, this is often a major issue they have to deal with everyday.

A third approach is then necessary that can ease the calling process, providing the localization of the caller inside the room. In this case, the person can even be lying down on the floor and thus, difficult to be tracked down by the robot when it gets into the room. By providing an accurate localization, the robot can travel directly to the place where the call was originated from. It can then proceed with any reconnaissance procedures in order to find the person in a shorter range.

This paper describes a method for calling a robot that can be easily used by elder people in any situation. It does not require batteries and provides sufficient accuracy of its localization in a room. It is based on a device (Click trainer) (Figure 1) that sends a high pitch mechanical tone when pressed and another when released. This system only uses sound waves as the high pitch tone propagates within the room walls. A method is described that uses the generated acoustic signal in order to track the caller's position.

Figure 1. Click device that produces a high pitch mechanical tone

Section II describes existing methods found in literature and Section III describes the objectives of this work, followed by some theoretical background on Section IV. Section V describes how the system was implemented and Section VI shows the methodology and obtained results in the experimentation, finishing with the conclusions on Section VII.

 ISBN: 978-1-61208-454-1

II. SOUND SOURCE LOCALIZATION

Tracking the localization of a sound source is an area of research that is well exploited. Authors have taken different approaches but the Time Difference of Arrival (TDOA) method is recurrently used. For that, an array of microphones is necessary and different authors use different methods and applications.

Mandlik [2] used an array of four microphones displaced in a square 1 m apart from each other in the center of a room (50 x 30 m). The sound of a speech is recorded by the microphones and then it is processed offline in order to calculate its source localization. The authors used signal processing, by using the Generalized Cross Correlation function (GCC), Fourier transform, Fourier transform filtering and Phase Transform filtering (PHAT), to estimate the time delay of the sound received between the four microphones. Based on the position of the microphones, a model was developed to estimate the 3D position of the sound source. According to the presented graphical results, the direction of the sound source was very accurate, although the position of the source (distance from the speaker to the microphone array) showed estimation points of up to 5 m apart from each other on the experimented results (~2.5 m error from the real speaker position).

Using TDOA and Direction Of Arrival (DOA), a group or researchers [3] developed an acoustic source localization system in order to trace sound at the band of 100 Hz to 4 kHz. Using two sets of microphone pairs (1 m apart) arranged on two perpendicular horizontal walls, they combined the two processes (TDOA and DOA) to estimate the time difference (on each microphone of a pair) with the angle (between pairs), thus providing a 2D position of the sound source. Signal processing is used such as Power Spectral analysis, Fast Fourier Transform and phase difference computation with a Finite Impulse Response filter. The presented experimental results show angle estimation errors (DOA) from 3º to 30º on the worst angle scenario (45º from the center of the microphone array), and errors below 1º for the best scenario (90º) with time delay differences of up to 0.2 ms for the various tested angles.

Combining signal processing (GCC and PHAT) on a TDOA system with the use of Artificial Neural Networks (ANN), a group of researchers [4] used an array of microphones to estimate the position and orientation of a sound source. Experimental results show estimation positional errors with an average of 0.341 m. With the application of a phase transform method they obtained positional errors with an average of 0.298 m in 3D space.

In general, it can be concluded that signal processing applied to an array of microphones and using the TDOA method, is the process many researchers implemented for sound source localization systems.

III. OBJECTIVES

By using the Click device of Figure 1, the objective is to locate its position when operated inside a room, as shown in Figure 2.

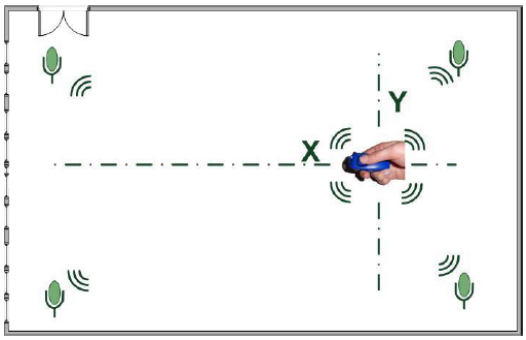

Figure 2. Click device localization when operated

A rectangular room was considered since it generalizes different room configurations (square, circular and rectangular). Four microphones were displaced in known positions of the room. They were placed near the corners and the ceiling since this was the best chance to avoid obstacles. Other configurations are planned to be experimented in the future, such as half way on each wall making a cross positioning. This paper only describes the results obtained with the microphones placed in corners.

Other two important objectives were defined: cost and accuracy. The system would have to be of low implementation cost for wide spreading in all rooms of nursing homes. The accuracy was defined to be less than 1 m radius around the caller, since it was considered sufficient for a good close visual detection of the caller from the robot.

IV. THEORETICAL BACKGROUND

Since this work uses sound waves, the first premise was the sound speed when propagating through air. At room temperature of 20º C the speed of sound is defined to be 343.21 m/s with 315.77 m/s at -25º C till 351.88 m/s at 35º C. When the sound is created in a certain spatial position, it is expected to travel in all directions at the same speed thus reaching each sensor (microphone) at a different time period. Sound waves at a temperature of 20º C take 2.91 ms to travel 1 m. If a sound starts at a distance of 1 m from one microphone and at 2 m from a second microphone there will be a difference of 2.91 ms of the sound arrival between microphones. This is TDOA as it is also graphically shown in Figure 3 (t_i and t_j is the time taken from the source s to microphones i and j respectively).

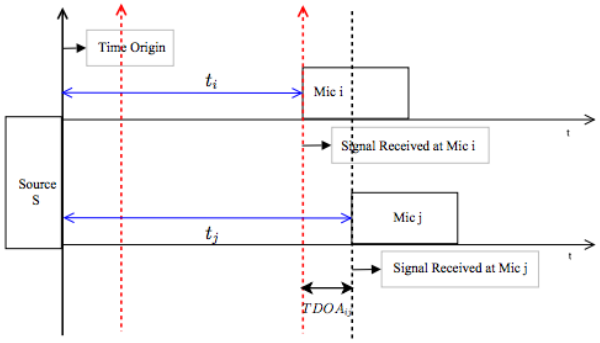

Figure 3. Signal receiving time in TDOA [5]

Although TDOA provides the time difference between two signals, it is still not a straight forward process to calculate the distance based on two microphones. There is no other way to communicate that a sound started at a given time. Therefore, one can only rely on the first samples of the sound signal, when they arrive, to start the clock ticking. An approach based on the TDOA is the DOA, or also Interaural Time Difference (ITD), which resembles the human ears. It provides the ability to track an angle where a sound is coming from. This angle (θ) is based on the distance that separates the two ears (x), the relative time difference of the sound arrival at the two ears (Δt) and the speed of sound (c), as shown in (1) [6].

$$\theta = \text{asin}\left(\frac{\Delta t\, c}{x}\right) \quad \textbf{(1)}$$

With the ITD angle calculated, it is then possible to compute the intersection between different angles in order to estimate a possible position of a sound source, as shown in the next section.

V. IMPLEMENTATION

Considering the ITD process, a pair of ears will be considered as a set of two microphones, separated by a x distance. Since four microphones are used near the corners of a rectangular room, each two microphones side by side will become 'ears' of that wall. In other words, a rectangular room will have then four sets of ears. Hence, four angles will be generated when a sound is created within the room, as shown in Figure 4.

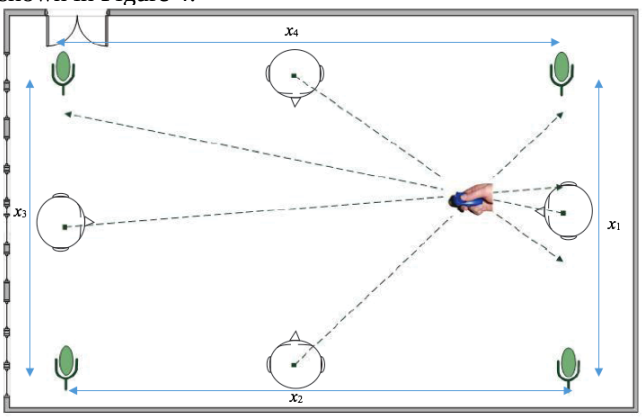

Figure 4. ITD process at work where each pair of microphones emulates the head ears with the different obtained angles from the sound source

After obtaining the θ angle for each pair of microphones, two points are then calculated. The first point (P_1) is on the "head" position (center point between two microphones). The second point (P_2) is obtained when the line crosses the opposite and parallel axis, as shown in Figure 5. This second point is obtained by multiplying the tangent of θ by the distance between the two parallel axes (x).

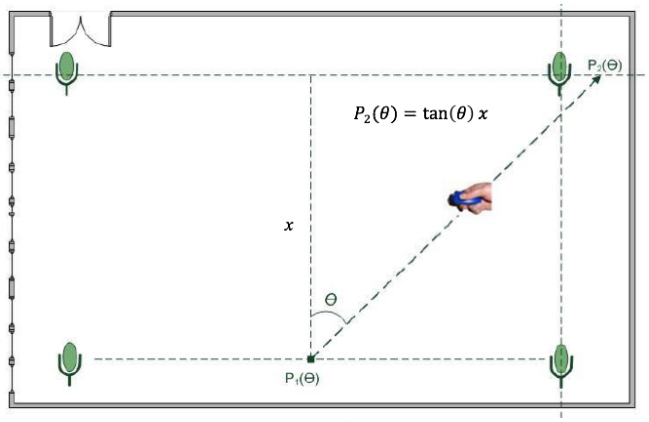

Figure 5. Obtaining P_2 from P_1 and θ angle

For each θ angle, two points are calculated and therefore, a total of height points (four lines) are obtained in the room. The intersection point between these four lines is the sound source (x, y) position. This point can be calculated using the determinant of each pair of lines, as shown in (2).

Considering a generic pair of obtained lines (lets call them line a and line b), points (x_1, y_1) and (x_2, y_2) are the points $P_1(\theta)$ and $P_2(\theta)$ of line a. Points (x_3, y_3) and (x_4, y_4) are the points $P_1(\theta)$ and $P_2(\theta)$ from line b. The point (P_x, P_y) is the intersecting point of line a and line b.

$$(P_x, P_y) = \left(\frac{(x_1y_2 - y_1x_2)(x_3 - x_4) - (x_1 - x_2)(x_3y_4 - y_3x_4)}{(x_1 - x_2)(y_3 - y_4) - (y_1 - y_2)(x_3 - x_4)}, \frac{(x_1y_2 - y_1x_2)(y_3 - y_4) - (y_1 - y_2)(x_3y_4 - y_3x_4)}{(x_1 - x_2)(y_3 - y_4) - (y_1 - y_2)(x_3 - x_4)} \right) \quad (2)$$

Although this intersection can be calculated from any pair of obtained lines, from experimentation, only two lines shown consistently lower deviations on the calculated position. They are the opposite lines from the closest microphone (opposite quadrant of the room) to the Click device (Figure 6). In practice the closest is the microphone that firstly receives the sound signal.

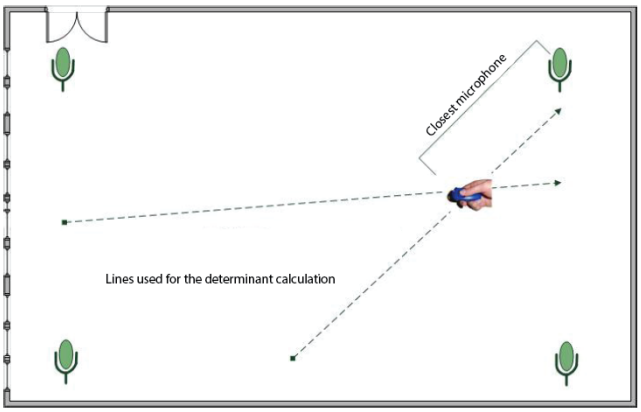

Figure 6. Closest microphone to the Click device and oposite lines used for the determinant calculation

 ISBN: 978-1-61208-454-1

Another important aspect on selecting the opposite quadrant, is the fact that on the same or adjacent quadrants, the line's intersection may produce a singularity: the lines are almost parallel to each other and therefore, an intersection point can fall outside the room. A small angle calculation deviation can move the intersection point outside the room, as shown in the example of Figure 7. This occurrence was found during trials.

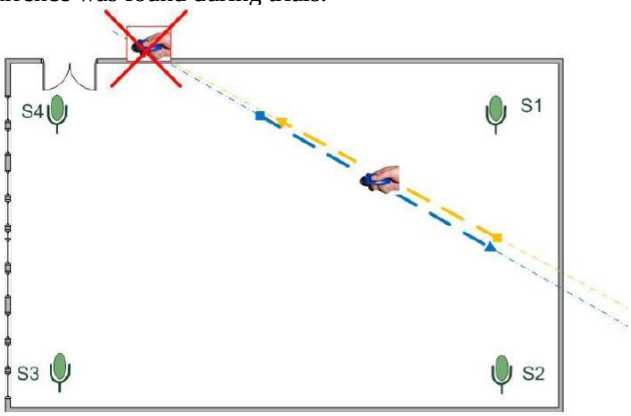

Figure 7. Example of an occurring singularity

The developed system was implemented in two separate blocks: Acoustic detection block (Adb) and Control block (Cb)(Figure 8).

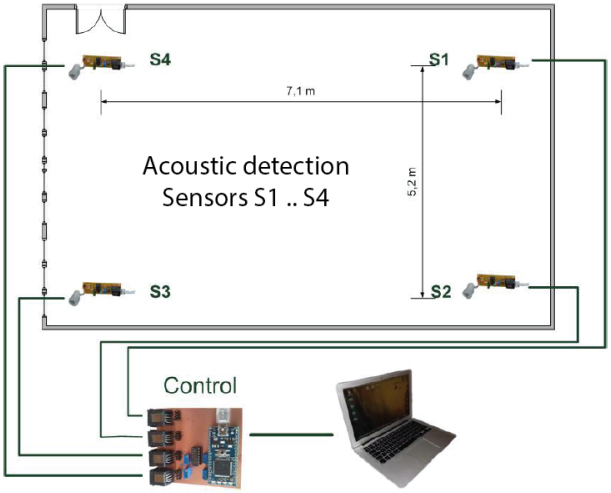

Figure 8. Developed system and the two blocks of operation

The Click device utilized on the experimental tests generates an acoustic tone at around 5 kHz (+/- 500 Hz). Each sensor (S1-S4) is based on an electret microphone with a pre-amplifier, a 2nd order high-pass filter tuned to 5 kHz, an amplifier and a threshold comparator. The latter produces the 5 V level pulses that are supplied to the Cb. These operations are performed by a single low cost chip with four operational amplifiers on the Adb side. More details of the developed system can be found in [7].

Each Adb is connected to the Cb via a twisted pair cable (Ethernet cable). The cable uses one pair for the signal (Adb to Cb) and one pair for powering the Adb (Cb to Adb).

The Cb contains an mbed NXP LPC1768 microcontroller board (ARM® Cortex™-M3 Core) with 96 MHz clock speed. It also contains a threshold comparator to regenerate the incoming signals from each sensor. These signals are then injected into four digital input ports of the microcontroller. At each incoming signal (pulsed signal as shown in Figure 9), a hardware interrupt is generated in the microcontroller that uses its internal timestamp to tag them. The timestamp is in microseconds. The system only reacts to the first pulse received per port and it ignores subsequent interrupts from the same port, until a valid point is calculated or a timeout is generated.

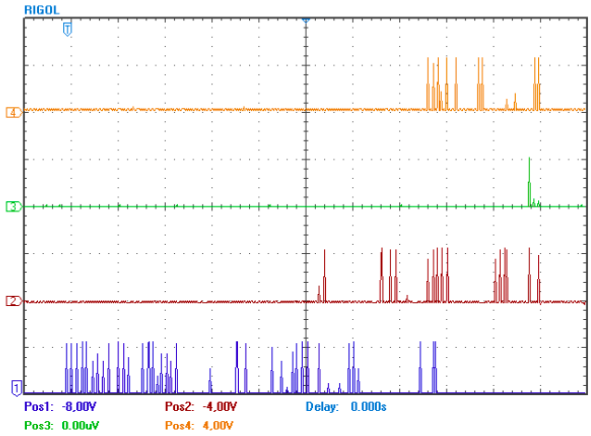

Figure 9. Example of obtained pulses on the four sensors and their time differences

After four valid signals are received, the microcontroller calculates the ITD angles. As explained before, the signals used are of the opposite microphones from the first received signal. From the angles, each line points (P_1 and $P_{2)}$ are calculated followed by the determinant of the pair of lines. The end result is the intersection point (P_x, P_y) that is sent to the robot via serial port of the microcontroller.

Room setup and sensor location information is configured in the microcontroller algorithms so the tracked position is relative to the real room length and width.

VI. EXPERIMENTATION

In order to test the accuracy of the developed system, trials were conducted where the Click device was positioned at different pre-determined positions in the room. A constant height of 1 m from the floor was used. On each position, three clicks were made at intervals of 2 s each. Figure 8 shows the room setup where the microphones are placed apart 7.1 m on the *x* axis and 5.2 m on the *y* axis. Two sets of tests were done on each round of trials: a) 12 positional diagonal points; b) 5 positional orthogonal points.

Figure 10 shows the results obtained on the diagonal trial positions. The blue diamond shape marks the intended real position where the clicks were performed. The obtained calculated positions are the other different encircled shapes where each circle is a set of three clicks. Figure 11 uses the same approach but for orthogonal trial positions from the sensors.

 ISBN: 978-1-61208-454-1

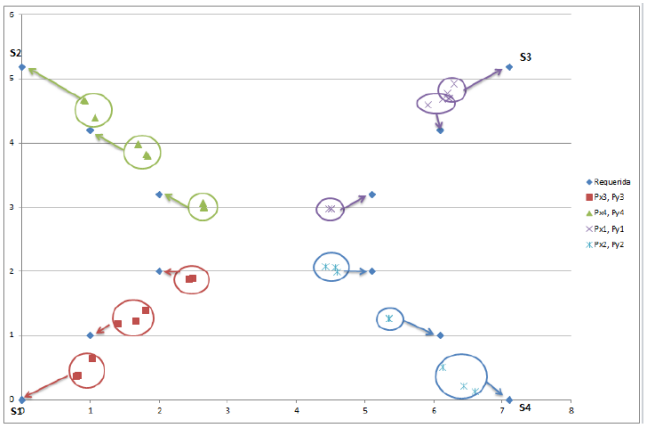

Figure 10. Trial results obtained at the diagonal of the sensors

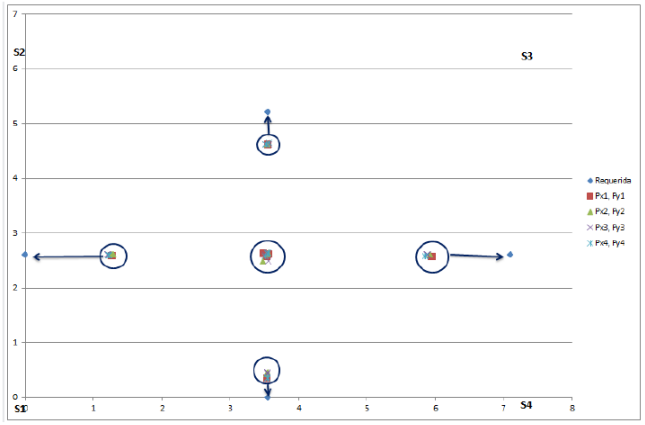

Figure 11. Trial results obtained at the orthogonal of the sensors

The results for the diagonal of the sensors show that, between each three clicks at the same position, a deviation of 0.229 m was found on the *x* axis and a deviation of 0.193 m was found on the *y* axis. For the positioning deviations on the diagonal tests, they were divided by quadrants and Table I summarizes the results.

TABLE I. STANDARD DEVIATION OF THE OBTAINED RESULTS

Quadrant	X(m)	Y(m)
1st	0.684523312	0.330336495
2nd	0.81212981	0.429232324
3rd	0.635961332	0.461925981
4th	0.913362087	0.706452613

The average deviation is then 0.761 m for the *x* axis and 0.482 m for the *y* axis. The absolute deviation (measured by the shortest distance between the real and the obtained points) is 0.901 m. For the orthogonal tests, the results demonstrated a lower deviation between each click on the same position (0.01 m), although they show a higher deviation on the *x* axis (1.191 m) and on the y axis (0.458 m). At the room center, the values were typically below 0.1 m. It is clear though, that as the Click device moves closer to a sensor, the deviation from the real value increases. On the other hand, as the device moves towards the quadrant borders, the values tend to be more consistent. They show very low differences at the same position, but a higher difference to the real value as it moves away from the center.

Another set of trials was conducted, in order to estimate the influence on the results of the Click device at different heights. Starting from the floor and with increments of 0.5 m up to a maximum of 2 m, tests were performed in the room center. This was where the lowest deviations were achieved at a fixed height of 1 m. At each height three clicks were performed. Table II shows the obtained deviation results in meters from the room center position (3.55 m, 2.6 m). As it is shown in the table, the influence of height in the deviation accounts for less than 5% in absolute terms and only in one axis.

TABLE II. TRIALS AT DIFFERENT HEIGHTS AND OBTAINED DEVIATION RESULTS

Height	$\overline{x}$	$\overline{y}$	*x* deviation	*y* deviation
0	3.57	2.66	0.02	0.06
0.5	3.56	2.59	0.01	-0.01
1	3.54	2.55	-0.01	-0.05
1.5	3.55	2.56	0.00	-0.04
2	3.55	2.53	0.00	-0.07

A descent trend in the obtained values is visible on the graph of Figure 12, from the floor level up to 1 m. Then, a levelling trend for heights above 1 m is achieved, showing that around this floor distance (1 m +/- 0.5 m) the best results are produced with the developed solution.

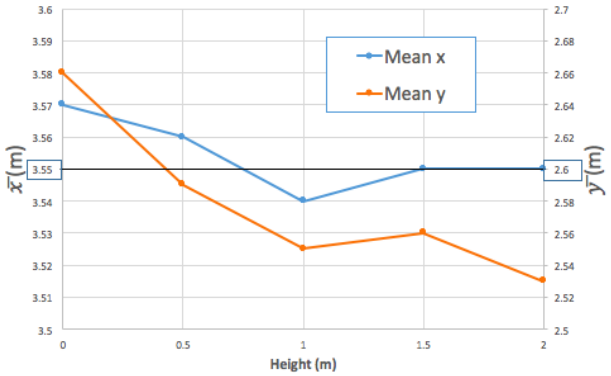

Figure 12. Trials graphical results at different heights

Further investigation is necessary in order to identify the influence of occlusions and reflections to the sound signal and the deviations caused by them.

VII. CONCLUSIONS

This paper presents a system for tracking the sound source localization of a Click trainer device. It describes a solution using simple and low cost devices that produces good results in terms of accuracy and simplicity. It has direct application on a robotic system's implementation, to localize a caller by an acoustic signal. The results show an accuracy below 1 m, fulfilling the original objective of localizing the person that called the service robot. The influence of the device position in height, showed a small deviation between the obtained position with the real one. Several improvements have to be addressed in the future, nonetheless

 ISBN: 978-1-61208-454-1

the achieved accuracy demonstrated other possible applications of the developed system in different areas.

REFERENCES

[1] RoboCup@Home. (2015, December 15). Retrieved from http://www.robocupathome.org/

[2] M. Mandlik and V. Brázda, "Sound source location method," Mandlik Magazines, vol. 6, nº 5, Dec. 2011, pp. 197-204.

[3] S. Paulose, E. Sebastian and B. Paul, "Acoustic Source Localization," International Journal of Advanced Research in Electrical, Electronics and Instrumentation Engineering, vol. 2, nº 2, Feb. 2013, pp. 933-939.

[4] A. Nakano, S. Nakagawa and K. Yamamoto, "Estimating the position and orientation of an acoustic source with a microphone array network," em INTERSPEECH 2009, 10th Annual Conference of the International Speech Communication Association, Brighton, United Kingdom, September 6-10, 2009, pp. 1127-1130.

[5] K. A. Tellakula, "Acoustic Source Localization Using Time Delay Estimation," Indian Institute of Science, Bangalore, India, 2007.

[6] R. M. Warren, "Auditory Perception," Cambridge University Press, Cambridge, UK, 2008.

[7] A. F. G. Albernaz, "Sistema de localização através de ondas de som no interior de edifícios," University of Minho, Guimaraes, Portugal, 2013.

 ISBN: 978-1-61208-454-1

Underwater Acoustic Physical Layer Emulator to Evaluate Digital Communications

M.S. Martins[ab], J. Cabral[a].

[a]CMEMS, University of Minho
Campus of Azurém, Guimarães, Portugal
[b]LARSyS, University of Algarve
Campus de Gambelas, PT-8005-139 Faro, Portugal
email: mmartins@dei.uminho.pt
cabral@dei.uminho.pt

G. Lopes[c], F. Ribeiro[c].

[c]Algoritmi Center, University of Minho, Campus of Azurém, Guimarães, Portugal
email: gil@dei.uminho.pt
fernando@dei.uminho.pt

***Abstract*—In order to achieve underwater acoustic high data-rate and real time communications, it is essential to implement a system that operates both at high and wideband frequencies using digital modulations. Therefore, to reduce the time and cost of developing acoustic communications an emulator of a physical layer model was implemented, allowing to test in real time the performance of digital modulations. The model was composed of an emitter transducer, a hydrophone and the subaquatic medium and was integrated in a Field Programmable Gate Array (FPGA) in order to emulate the physical layer in the acoustic modem testing. The emitter transducer and the hydrophone models were designed to meet real prototype characteristics. The system prototype was implemented in order to compare the experimental trials results with those obtained in emulator, emulating the transmission of acoustic signals, using different types of digital modulations. The system was tested using Binary Phase-Shift Keying (BPSK), Binary Frequency Shift keying (BFSK) and Binary Amplitude Shift Keying (BASK) modulations with a 1 MHz carrier frequency resulting in a data rate of 125 kbps. It was verified that the implemented model represents a suitable approximation to the real subaquatic communication channel, allowing the evaluation of digital acoustic communications.**

Keywords-Underwater Digital Communications; Acoustic Transducer Simulation; Acoustic Communications Emulator.

I. INTRODUCTION

Underwater wireless communications are a decisive technology for underwater sensor networks, divers and submarine communications, robotics and Autonomous Underwater Vehicle (AUVs) navigation and control.

Therefore, it is imperative to find reliable solutions, able to fulfill all these needs. There are three main forms to communicate through water: acoustic, radio frequency and optical [1]. Radio frequency is limited by the high level of absorption in water [2]. Optical systems suffer from the same limitation as well as the disadvantages associated to the high levels of ambient light close to the water surface and scattering due to suspended particles [3]. As a result, acoustic communication systems are the preferential form of wireless underwater communications, since they show low sound attenuation in water [4]. Acoustic communications have been used for long distance communications, up to 20 km, and in deep waters with stable thermal conditions. But, despite underwater wireless communications having shown strong advances in recent years, there are still many limitations concerning data rates and robustness for real-time applications [5].

There are several solutions to increase the modulation efficiency or data rate. The most used solutions are: increasing the carrier frequency [6] or increasing the symbol rate per carrier period [7].

High frequencies also raise strong problems related to attenuation. Being directly related to the frequency, the acoustic absorption at 1 MHz can reach 280 dB/km [13]. Consequently, the maximum communication range decreases dramatically to a few hundred meters or less with the increasing of frequency [8]. On the other hand, real time acoustic communications are not supported at long distances, since acoustic waves propagate at around 1500 m/s, resulting in high propagation delays and disabling, therefore, any real time connection [8]. Therefore, high data rate transmissions are only reliable for short and medium distances.

There are works showing that it is possible to use frequencies up to 1 MHz to achieve high data rate acoustic communications. For example, in [9] the authors presented an acoustic FPGA based on a modem operating at frequencies between 100 kHz and 1 MHz, for distances ranging between 50 m and 100 m. Using a BPSK modulation with a 800 kHz carrier frequency, the system archived a 80 kbps data rate.

In the previous work the authors presented an underwater low power acoustic modem to operate over tens of meters, achieving a maximum data rate of 1 Mbps using carriers up to 1 MHz [10] [11].

However, the development of acoustic technology for underwater applications consumes high amounts of time and resources. Therefore, the proposed emulator allows a rapid development and test of acoustic modems. Allowing in the test digital modulations performance before implementing in a field, helping in the selection the most reliable solutions reducing the development time and cost. To do so, it was necessary to implement a communication system composed by an emitter transducer, a hydrophone and the corresponding conditioning electronics to experimentally validate the emulator results. The underwater channel model was implemented and tested in shallow waters, including MHz frequency range, directional spreading type, attenuation, ambient noise, Doppler Effect, propagation delay and multipath. To complete the system it was necessary to implement a model for piezoelectric

 ISBN: 978-1-61208-454-1

transducers. The selected emitter was a homemade Piston type transducer for a directional beam. The hydrophone was a commercial transducer Cetacean ResearchTM C304XR with linear response (±3dB) for a frequency range between 0.012 and 1000 kHz [12].

In Section 2, a small physical proprieties background of the underwater acoustic channel and ultrasonic transducer is introduced. In Section 3, the experimental setup is presented and, in Section 4, the physical layer emulator implementation is described. Section 5, present the results of the emulator model evaluation and the comparisons with real trials. Finally, in Section 6, conclusions and future work are presented.

II. PHYSICAL LAYER BACKGROUD

The underwater acoustic communication physical layer is composed by the emitter ultrasonic transducer, hydrophone and the subaquatic medium. To allow a better understanding of the underwater acoustics, this section will present the physics background of the ultrasonic transducer and subaquatic medium.

A. Underwater Acoustic Channel

Despite the advantages of acoustic communication in underwater environments, when compared to optical and radio, the propagation of sound also has significant challenges that influence the development of underwater acoustic communication systems. This is mainly due to the slow speed of acoustic propagation in water (about 1500 m/s). When studying sound propagation in the underwater acoustic channel, some relevant phenomena must be taken into account: attenuation, ambient noise, Doppler Effect, propagation delay and multipath [8].

B. Ultrasonic transducers

The ultrasonic transducers are commonly made using piezoelectric materials, because they present good response to high frequencies. The ultrasonic transducers convert the electric energy into sound and vice versa [13]. Therefore, to implement an ultrasonic transducer model it is necessary to comprehend piezoelectric material response and behavior. There are several factors that influence the transducer performance, namely the structural damping, acoustic impedance mismatch and electrical damping [14]. Structural damping is due to the energy dissipation and reaction time in the geometrical deformations of the transducer when the electrical field is applied. The acoustic impedance mismatch, between the transducer and the medium, causes acoustic waves to be reflected back to transducer. The resonance transducers are designed to overcome this fact, since the internal acoustic waves are synchronized with the electrical drive signal, causing an addition of the two signals and therefore increasing the output. Electrical damping is due to transducer capacitor effects which result in a time lag between the application of the electrical signal and the transducer response. However, this effect can be corrected by implement an impedance matching circuit, therefore this matter will not be addressed in this document.

Piezoelectric ultrasound transducers, at high frequencies, usually operate in the 33 mode, that is, the deformation along the polarization axis and the excitation electric field point into the same direction. Consequently, in this work, it will only be addressed the piston type transducer operating in thickness mode. The free displacement of the material in direction 3, without restraining force and assuming uniform strain over the surface [14], is given by:

$$\xi = nvd_{33} \tag{1}$$

where ξ is the free displacement, v is the applied voltage, d_{33} is the coupling coefficient in the thickness direction and n is the number of layers.

The displacement is also dependent on the stress and strain of the viscoelasticity of the piezoelectric material, resulting in a structural damping. When an electric field is applied to the polymer charged particles, they move inside the actuator to align the charges. In this process, some of the energy is dissipated and the reaction time is also affected. The final displacement for a piezoelectric stack transducer, operating in the 33 mode, can be written as a function of the nondimensional frequency [14]:

$$\frac{u(\sigma)}{u_{st}} = \frac{RC_p^S\omega_m\sigma + 1}{(\sigma^2+1)(RC_p^S\omega_m\sigma+1) + k_{33}^2 RC_p^S\omega_m\sigma},$$

$$\sigma = \frac{s}{\omega_m} \tag{2}$$

where σ is the nondimensional frequency in which 1 represents the short circuit mechanical resonance, R is the shunt resistance, C_P^S is the stain-free capacitance, ω_m is the short circuit mechanical resonance and k_{33}^2 is the generalized piezoelectric coupling coefficient. The ω_m and k_{33}^2 can be calculated with (3) and (4), respectively.

$$k_{33}^2 = 1 - S_{33}^E \varepsilon_{33}^T \tag{3}$$

$$\omega_m = \frac{k + k_a^E}{m} \tag{4}$$

k is the viscoelastic stiffness, k_a^E is the short circuit stiffness of the actuator, m is the actuator mass and ε_{33}^T is the stress free dielectric permittivity.

Another important aspect is related to the transducer acoustic impedance. The sound wave created inside the transducer reflects, in part, at the boundary established by different densities and bulk modulus B of the transducers and the medium according to the Snell's law [15]. This reflection creates deformations on the acoustic signal transmitted to the medium [13], which can be calculated by:

$$a_{out}(t) = lt_w\left(a_{in}(t) + r_w a_{in}(t + D_p)\right) \tag{5}$$

Converting to the Laplace domain we obtain the following transfer function:

$$\frac{A_{out}(s)}{A_{in}(s)} = LT_w\left(1 + R_w e^{sDp}\right) \quad (6)$$

Here, a_{out} is the sound wave output as function of time t, a_{in} is the sound wave as function of time created inside the active element, t_w is the transmitted sound wave intensity percentage, r_w is the reflected sound wave intensity percentage, l is the internal acoustic energy loss and D_p is the delay of the reflected sound wave, introduced by the active element thickness.

III. EXPERIMENTAL SETUP

In order to achieve high data-rate communications, it was essential to implement a system prototype that operates at high frequencies (up to 1 MHz). The acoustic system was designed to be reconfigurable and reprogrammable, over dimensioning all parts of the system allowing future upgrades.

A. Acoustic Modem

In order to design an acoustic modem capable of performing several types of digital modulations, a highly adaptable system was developed.

The acoustic modem was implemented in a Xilinx Spartan-3A, which is responsible for modulation and demodulation, control of the receiver instrumentation and output amplifiers. The system runs with an external clock of 50 MHz. The receiver is composed in this order by 100kHz High Pass Filter, which removes all the low frequency noises, a variable gain control amplifier, from -22 to 20 dB, a Antialiasing filter and an ADC AD9244. To driver signals at the output of the FPGA modulator a DAC DAC904 and a Class B Push-Pull symmetric voltage amplifier were implemented with a of 12 dB gain. The ultrasonic emitter was a homemade PZT-5H 2 mm piston type transducer with 2 cm diameter [16]. Despite the transducer's directionality, a residual pressure wave projected in the transducer rear can achieve 15% of the main front pressure wave amplitude. The ultrasonic receptor used to register the pressure waves was the Cetacean ResearchTM C304XR hydrophone, with a transducer sensibility of -201 dB, re 1 V/µPa and a linear Frequency Range (±3dB) of 0.012–1000 kHz. The filter block consists of a 2nd order band-pass filter from 0.001 to 2 MHz with a gain in the pass band of 6dB. The digital oscilloscope used to record the measurements was a PicoScope 4227 100 MHz.

IV. PHYSICAL LAYER EMULATION SYSTEM

The physical layer emulator allows testing the acoustic modem performance for different types of digital modulations without physical implementation. This process reduces the cost and time spent. The emulator consists in a computer model for all physical layers blocks to be integrated in the FPGA program. Therefore the FPGA, in addition to modulate and demodulate functions, still emulates the acoustic modem electronics and the subaquatic medium, as presented in Figure 1.

The modulator and demodulator were implemented according to the selected type of modulation: BPSK, BFSK and BASK. Since, the emulator model was implemented in a discrete algorithm (Z-Transform), it was not necessary to implement the analog to digital and digital to analog converters (ADC and DAC) blocks.

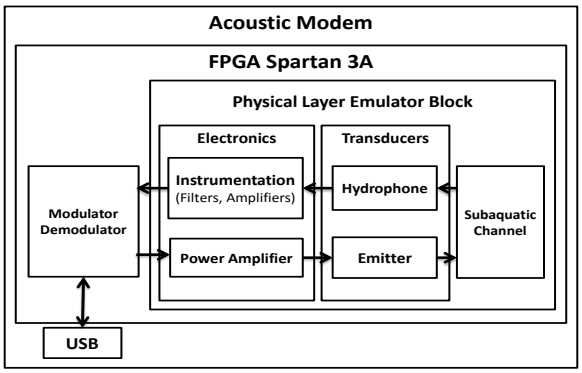

Figure 1. Physical layer emulation blocks.

The algorithm is divided in three parts: the electronics model, the transducer and channel model. The electronics model is a fixed model where is not necessary to define any variables, since electronics circuits model (instrumentation and power amplifier) were implemented using digital filters according to the correspondent transfer function available in each component datasheet. The transducer and the channel model are user defined models where is necessary to define the system variables such as: transducer characteristics (mechanical and electrical characteristic), medium characteristics (temperature, salinity, acidity, shipping factor and wind speed) and the scenario setup (dimensions, hydrophone position, emitter position, reference distance, hydrophone and emitter velocity relative to the medium).

V. RESULTS

This section shows the results obtained in the experimental tests in order to compare them with those obtained by the emulator.

The experimental analysis tested the attenuation, multipath and transducer response to digital modulations. The Doppler Effect and noise was discarded. This decision was justified by the great difficulty in assembling an experimental setup with moving parts in the medium and at 1 MHz the underwater environment is relatively silent.

A. Attenuation

The swimming pool was 12 m long, 4 m wide and 3 m deep. Four test distances were defined: 1, 4, 8 and 12 m, where measurements were performed at 50 cm deep and in the middle of the pool (2 m either side). At each distance, several frequencies were tested: 100 kHz, 200 kHz, 300 kHz, 400 kHz, 500 kHz, 600 kHz, 700 kHz, 800 kHz, 900 kHz, 1 MHz, 1.2 MHz and 1.4 MHz.

The simulation was configured with the conditions observed in the experimental tests, with fresh water at a temperature of 13 ºC and 7.2 pH.

 ISBN: 978-1-61208-454-1

The projector and the hydrophone sound wave level responses are irrelevant since the considered results are relative. A reference measurement was taken at 10 cm intervals over several distances for all the tested frequencies and attenuation, and calculated according to the following equation:

$$20\log_{10}\left(\frac{p}{p_{ref}}\right) \quad (7)$$

where $\boldsymbol{p}$ is the value of the pressure wave at the receiver and the $\boldsymbol{p_{ref}}$ is the value of the pressure wave at the reference distance. The experimental values are presented as an average of 10 measurements, with a maximum error of 3.5%.´

Figure 2 shows that attenuation increases with the increasing distance. The 1 MHz point shows a low attenuation peak in all the curves that gets smoother with the increasing distance. This fact is related to the emitter optimal frequency (resonance point). Moreover, attenuation does not increase with the increasing frequency as the beam divergence angle decreases with frequency.

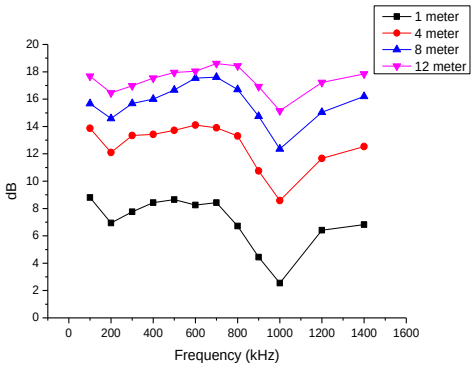

Figure 2. Experimental attenuation results as a function of frequency.

The simulation (Figure 3) shows the overall results with lower attenuations, but the general trend is similar to that obtained with the experimental results. The resemblance between the two curves increases with the increasing distance.

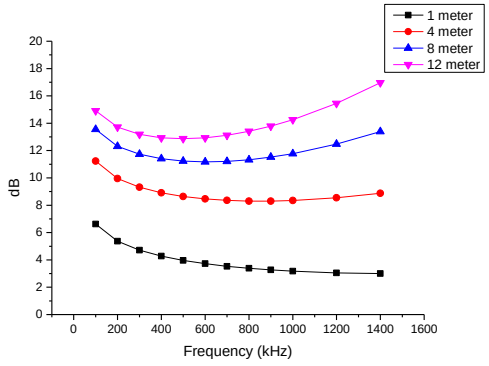

Figure 3. Emulatior attenuation results as a function of frequency.

The difference between the experimental and the simulated results assumes an average of 3.2 dB reaching a 6 dB peak. This difference occurs because the used model was developed for a range of kilometers rather than meters and the low attenuation peak at 1 MHz in all the graphics is due to the transducer optimal operational frequency.

B. Multipath

The multipath performance was also evaluated in the pool were a burst signal of 20 cycles at 1 MHz, over a distance of 12 m was transmitted. The ultrasonic emitter and hydrophone positions were (0.03; 1.95; 0.5) and (11.61; 1.95; 0.5) meters. At this frequency, both the emitter and the hydrophone operate in a directional pattern.

Figure 4 shows the experimental results for the second configuration.

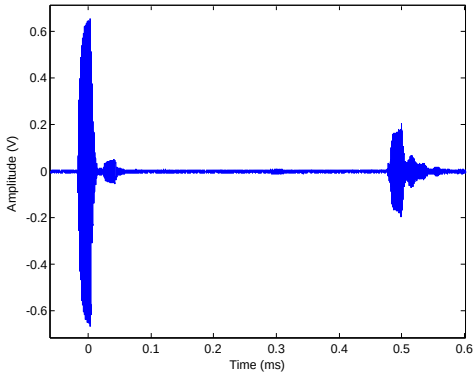

Figure 4. Multipath signal received from a burst signal of 20 cycles at 1 MHz over 12 meters.

Figure 4 also shows three sets of signals. At 1 MHz the transducer was operating in a directional pattern with a divergence angle of 4.3º and, therefore, only the back and front echoes appear in the results.

The first set is from the direct path, the second is from the back echo and the third is from the front echo. The back eco has lower amplitude than the front echo, despite traveling a shorter distance. This is due as the back echo results from a residual energy loss in the rear part of the transducer.

Figure 5 shows the emulation results for the second configuration.

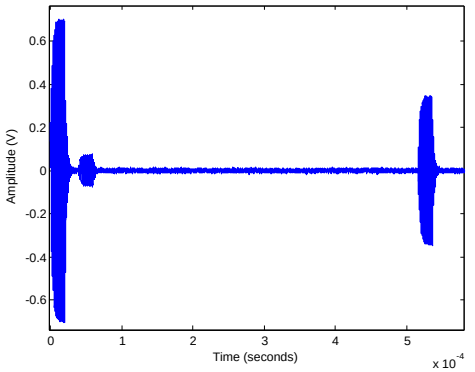

Figure 5. Multipath emulation of a burst signal of 20 cycles at 1 MHz over 12 meters.

 ISBN: 978-1-61208-454-1

The emulator achieves a good approximation to the real-world case, with similar phase and amplitude distortion, despite the simulation only including the 1st order echoes.

C. Transducers response to digital modulation

In order to evaluate the performance of ultrasound transducers, using digital modulations, fundamental modulations such as BPSK, BFSK and BASK were considered [17]. The carrier frequency was set to 1 MHz with a 125 kbps baud rate.

Figures 6, 7 and 8 show the transducer's behavior to the BPSK, BFSK and BASK modulations, respectively. Each figure shows the modulation signal, the FPGA emulation and the real test signal.

Figure 6c shows the BPSK modulation, where the 180º phase shift corresponds to the logic level transition. The PZT transducer shows a high damping effect duo to the energy stored inside the transducer. In the moment of phase shit the two signals try to cancel one another.

In the BFSK drive signal of Figure 7 the high logic level '1' and the low logic level '0' were modulated with carriers of 1 MHz and 500 kHz, respectively. In the FSK modulation, the carrier frequencies are usually adopted with close values, but, in order to simplify the evaluation, the option of using two very distinct frequencies was taken. The 500 kHz frequency is highly attenuated due to two factors, the first is that the transducer acoustic output is proportional to the frequency, resulting in half amplitude and, the second is that the transducer was projected to operate at maximum optimization point at 1 MHz.

In the BASK, the low logic level was set to half of the high logic level amplitude, as presented in figure 8a. Similar to the BFSK test, the transducer shows also a high damping effect resulting in slow amplitude variations.

Comparing Figures 6b, 7b and 8b with the Figures 6c, 7c and 8c it is possible to observe the similarity between emulations and real tests, confirming the suitability of the developed model.

VI. Conclusions and Future Work

A physical layer FPGA based emulator for underwater acoustic communications was developed. The model was designed specifically to emulate the acoustic channel and ultrasonic transducers, allowing performance evaluation for of the ultrasound communications using digital modulations.

The acoustic underwater communication channel model was taking into account several phenomena: attenuation, multipath, environment noise and propagation delay. Real tests were also implemented to validate the attenuation, multipath and propagation delay.

The transducer models, using digital modulations, were simulated and validated with real tests. The results show that the transducer models present a similar response to real tests.

Overall, the results show that the model represents a useful approximation to the real subaquatic communication channel, being therefore an important tool to simulate the propagation of acoustic signals.

In future works, we will implement and test a communication using Frequency Division Multiplexing (FDM) modulations in order to achieve data rates in the order of 1.5 to 2 Mbps.

Acknowledgment

M. S. Martins thanks the FCT for the Post-Doctoral fellowships grant SFRH/BPD/107826/2015.

References

[1] M. Chitre, S. Shahabudeen, and M. Stojanovic, "Underwater Acoustic Communications and Networking: Recent Advances and Future Challenges," *Mar. Technol. Soc. J.*, vol. 42, no. 1, pp. 103–116, Mar. 2008.

[2] X. Che, I. Wells, G. Dickers, P. Kear, and X. Gong, "Re-evaluation of RF electromagnetic communication in underwater sensor networks," *IEEE Commun. Mag.*, vol. 48, no. 12, pp. 143–151, Dec. 2010.

[3] G. Baiden, Y. Bissiri, and A. Masoti, "Paving the way for a future underwater omni-directional wireless optical communication systems," *Ocean Eng.*, vol. 36, no. 9–10, pp. 633–640, Jul. 2009.

[4] I. F. Akyildiz, D. Pompili, and T. Melodia, "Underwater acoustic sensor networks: research challenges," *Ad Hoc Networks*, vol. 3, no. 3, pp. 257–279, May 2005.

[5] S. Roy, T. M. Duman, V. McDonald, and J. G. Proakis, "High-Rate Communication for Underwater Acoustic Channels Using Multiple Transmitters and Space–Time Coding: Receiver Structures and Experimental Results," *IEEE J. Ocean. Eng.*, vol. 32, no. 3, pp. 663–688, Jul. 2007.

[6] N. Nowsheen, C. Benson, and M. Frater, "Design of a high frequency FPGA acoustic modem for underwater communication," in *OCEANS'10 IEEE SYDNEY*, 2010, pp. 1–6.

[7] J. Huang, S. Zhou, and Z. Wang, "Performance Results of Two Iterative Receivers for Distributed MIMO OFDM With Large Doppler Deviations," *IEEE J. Ocean. Eng.*, vol. 38, no. 2, pp. 347–357, Apr. 2013.

[8] M. Stojanovic and J. Preisig, "Underwater acoustic communication channels: Propagation models and statistical characterization," *IEEE Commun. Mag.*, vol. 47, no. 1, pp. 84–89, Jan. 2009.

[9] N. Nowsheen, C. Benson, and M. Frater, "A high data-rate, software-defined underwater acoustic modem," in *OCEANS 2010 MTS/IEEE SEATTLE*, 2010, pp. 1–5.

[10] M. S. Martins, N. Pinto, J. P. Carmo, and J. Cabral, "High data rate acoustic modem for underwater aplications," in *2014 International Telecommunications Symposium (ITS)*, 2014, pp. 1–5.

[11] M. S. Martins, N. Pinto, G. Rocha, J. Cabral, and S. Laceros Mendez, "Development of a 1 Mbps low power acoustic modem for underwater communications," in *2014 IEEE International Ultrasonics Symposium*, 2014, pp. 2482–2485.

[12] "Cetacean Research Technology." [Online]. Available: http://www.cetaceanresearch.com/hydrophones/c304-hydrophone/index.html.

[13] C. H. Sherman and J. L. Butler, *Transducers and Arrays for*

 ISBN: 978-1-61208-454-1

Underwater Sound. Springer Science+Business Media, LLC, 2007.

[14] D. J. Leo, *Engineering Analysis of Smart Material Systems*. John Wiley & Sons, Inc., 2007.

[15] K. B. Wolf and G. Krotzsch, "Geometry and dynamics in refracting systems," *Eur. J. Phys.*, vol. 16, no. 1, pp. 14–20, Jan. 1995.

[16] M. Martins, V. Correia, J. M. Cabral, S. Lanceros-Mendez, and J. G. Rocha, "Optimization of piezoelectric ultrasound emitter transducers for underwater communications," *Sensors Actuators A Phys.*, vol. 184, pp. 141–148, Sep. 2012.

[17] C. Erdogan, I. Myderrizi, and S. Minaei, "FPGA Implementation of BASK-BFSK-BPSK Digital Modulators [Testing Ourselves]," *IEEE Antennas Propag. Mag.*, vol. 54, no. 2, pp. 262–269, Apr. 2012.

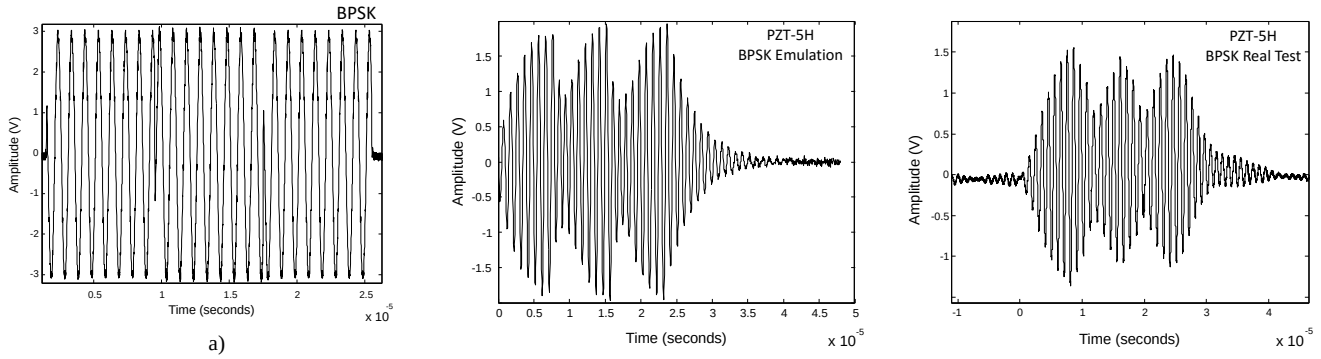

a) b) c)

Figure 6. BPSK modulation signal (a), FPGA emulation (b) and real test signal (c).

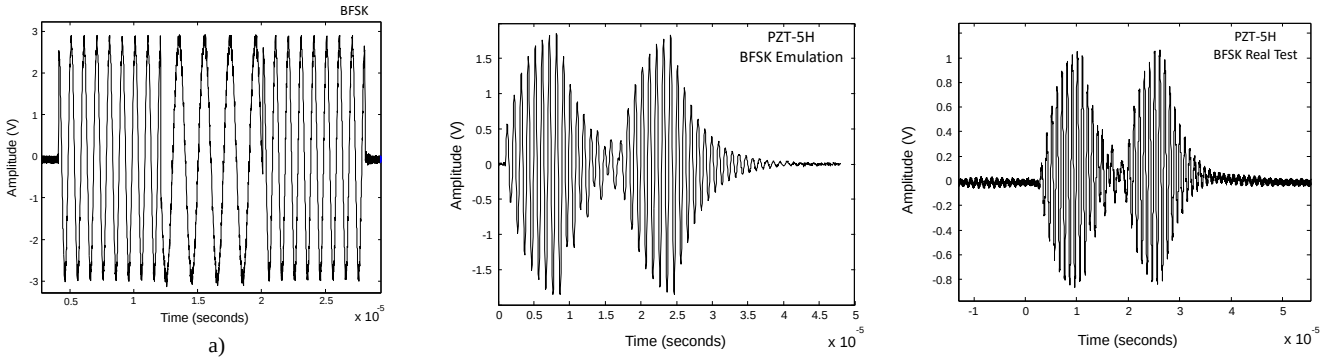

a) b) c)

Figure 7. BFSK modulation signal (a), FPGA emulation (b) and real test signal (c).

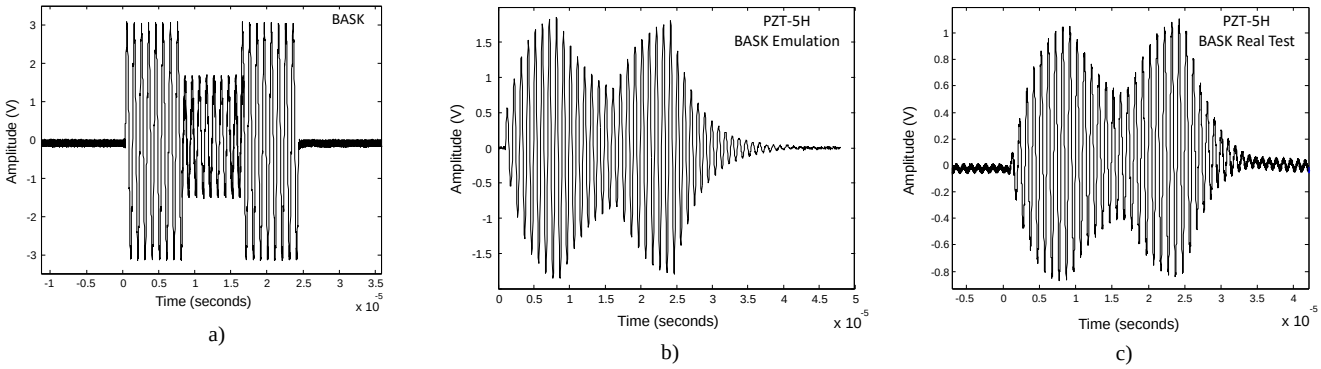

a) b) c)

Figure 8. BASK modulation signal (a), FPGA emulation (b) and real test signal (c).

QoS Control Method for W-LAN Ad Hoc Network With Automatic Contention Window Adjustment

Masaki Hanada, Moo Wan Kim
Tokyo University of Information Sciences
Chiba, Japan
e-mail : mwkim@rsch.tuis.ac.jp

Hidehiro Kanemitsu
Waseda University
Tokyo, Japan
e-mail : Kanemih@ruri.waseda.jp

Kazuo Hajikano
Daiichi Institute of Technology
Kirishima, Japan
e-mail : k-hajikano@daiichi-koudai.ac.jp

Hee-Dong Kim
Hankuk University of Foreign Studies
Yongin, Korea
e-mail : kimhd@hufs.ac.kr

***Abstract*—This paper proposes a new QoS control method for the ad hoc Wireless LAN (W-LAN), which adjusts the Contention Window (CW) size dynamically based on the required and achieved bit rate. By the proposed method, a node with higher bit rates can have better chance to send the data in order to satisfy the Quality of Service (QoS) requirement. This paper also shows the effectiveness of the proposed method based on the results of computer simulations.**

Keywords-QoS; IEEE802.11b/a; Ad Hoc Network; Contention Window; Required Bit Rate

I. INTRODUCTION

With the increase in the demand of multimedia communications in the area of wireless networks, a number of studies about the Quality of Service (QoS) control have been performed [1]-[10]. Especially, Wireless LAN (W-LAN) has been expected to be an important communication technology because new high speed specifications have been realized continuously. IEEE802.11, the standard of W-LAN, has a Distributed Coordination Function (DCF) access method. DCF is based on Carrier Sense Multiple Access with Collision Avoidance (CSMA / CA) and its outline is as follows:

(1) When the sender node attempts to transmit a frame, it first senses the channel status.
(2) If the channel is idle during the period of Distributed Inter Frame Spacing (DIFS), the sender node transmits the frame.
(3) If the channel is busy, then the sender node waits until the channel becomes idle. After the channel becomes idle, it still waits for the period of DIFS. Then, it determines the back-off time defined within the Contention Window (CW) which is necessary to reduce collisions.
(4) When the back-off time reaches zero, then the sender node starts to transmit the frame and the destination node replies with an Acknowledgment (ACK) to the sender node after waiting for the period of Short Inter Frame Spacing (SIFS).

In this procedure, all nodes have statistically equal probability to acquire transmission opportunity. So, IEEE 802.11 defines a QoS framework called Enhanced Distributed Channel Access (EDCA) which changes the CW size based on four traffic access categories, namely, Voice, Video, Best Effort Data and Background Data. Voice traffic has the smallest CW after collision or completion of previous transmission. But EDCA does not include any consideration about the difference of node's required bit rate.

There are several studies regarding QoS of IEEE802.11. The paper by L. Romdhani et al. [8] proposed Adaptive EDCF (AEDCF) for ad hoc networks, which gradually adjusts the expansion rate of the CW after collision and diminishes the rate of CW after successful transmission. DCF and EDCA are known to work relatively well when the traffic load is not so heavy, but when the medium is saturated, they no longer work effectively because EDCA does not have a mechanism to alleviate collisions. AEDCA works 25% better in high traffic load conditions than EDCA by simulation. Another paper by J. Maeda et al. [9] proposed to change the CW based on the required bit rate and frame size. This assumes the Access Point (AP) collects the required bit rates and calculates the CW for each node.

We propose a similar strategy to [9] and we introduce a required bit rate driven CW adjustment. The CW is updated dynamically by the achieved bit rate [10]. We expect this feedback mechanism to contribute to a fairness of bandwidth allocation by taking the actual network conditions into account.

The rest of this paper is organized as follows. Section II describes the proposed QoS control method. Section III shows the effectiveness of the proposed method based on the evaluation result. Section IV describes the conclusion of this paper.

II. PROPOSAL OF QOS CONTROL METHOD

In the CSMA/CA procedure, the back-off time is determined as follows:

Back-off Time = Random () * Slot Time

 ISBN: 978-1-61208-454-1

Random ( ) is the function to generate a random number of integer values based on the uniform distribution in the range [0, CW].

The main purpose of proposed method is to make the following Achievement Ratio equal, as much as possible, for nodes requiring different bit rate.

$$\text{Achievement Ratio} = \frac{\text{Achievement throughput}}{\text{Requited throughput}}$$

Let us consider the example of two nodes, where the requirement bit rate of node 1 is twice as large as the required bit rate for node 2. In case of the standard method, the Achievement Ratio of node 1 is higher than that of node 2 because the standard does not have any method to consider the difference of the node's required bit rate. So, our proposal is based on the idea that the value of CW is determined by considering the difference of the required bit rate and it is also changed adaptively based on the transmission result (e.g., successfully transmitted frame number).

The CW for node i after time d (i.e., CWi (t+d)) is determined by (1).

$$CWi\ (t+d) = CWi\ (t) + (FSi - Fi)*FL / (Fi*ST) \quad (1)$$

where
FL = Transmission time of one frame
ST = Slot Time
Fi = Target transmission frame number of Node i during time d which is calculated by (2)
FSi = Successfully transmitted frame number of Node i during time d

In (1), Fi is defined as follows:

$$Fi = \sum_{J} (Tj * Ri * FSi) / (Rj * Ti) \quad (2)$$

where
T_i = Achieved throughput of Node i
R_i = Required throughput of Node i

Equations (1) and (2) present the algorithms used to adjust CW. Each node in the network notifies the other nodes of its values for CW/ required bit rate/achieved bit rate before starting communication. Then, all nodes determine their CW (t+d) by (1), and start communication based on CSMA / CA procedure. Therefore, by the back-off time control of the proposed method, the back-off time of the node with lower required bit rate will be longer and the back-off time of the node with higher required bit rate will be shorter.

III. COMPUTER SIMULATION

A. Simulation Method

Computer simulation has been performed to evaluate the proposed method based on IEEE802.11b and 11a. Table 1 shows the network parameters. Nominal Maximum Throughput is the maximum transmission rate by the IEEE standard and any other parameters follow standard unless it is explicitly mentioned. Frame generation for each node is assumed to follow the Poisson distribution.

Two groups of nodes have been assumed, and each group has 10 nodes. All nodes in Group 1 share the same throughput requirement and Group 2 also share the same throughput which is twice higher than Group 1. Table 2 for 802.11b and Table 3 for 11a show the simulation cases from light load to very saturated load. The Required Throughput per Node is the generated throughput at each node of each group. The Total Load is the sum of these generated throughputs. In these simulations, a total of 20 nodes built one ad-hoc network. Any node is in radio ranges of all other nodes, so there are no hidden nodes and RTS/CTS are not applied. These simulations assume ideal radio environment without any interferences or background noise. Also, it does not consider free space loss of radio propagation. This simulation is intended to evaluate the proposed MAC layer mechanism.

TABLE 1 NETWORK PARAMETERS

IEEE 802.11 Standard	**11b**	**11a**
Mode	Ad-hoc	Ad-hoc
Nominal Max. Throughput (Mbps)	11	54
SIFS Period (μsec)	10	16
DIFS Period (μsec)	50	34
Slot Time (μsec)	20	9
CW Max	1023	1023
CW Min	31	15
Frame Size (byte)	1000	1000
Simulation Time (sec)	60	60

TABLE 2 SIMULATION CASES PARAMETER FOR 802.11b

802.11b		**Case 1**	**Case 2**	**Case 3**	**Case 4**
Required Throughput per Node (Mbps)	Group 1	0.2	0.3	0.36	0.5
	Group 2	0.4	0.6	0.72	1
Nominal Max. Throughput (Mbps)		11	11	11	11
Total Load (Mbps)		6	9	10.8	15
Load Ratio		0.545	0.818	0.982	1.364

 ISBN: 978-1-61208-454-1

TABLE 3 SIMULATION CASES PARAMETER FOR 802.11a

802.11a		Case 1	Case 2	Case 3	Case 4
Required Throughput per STA (Mbps)	Group 1	1	1.5	1.8	2
	Group 2	2	3	3.6	4
Nominal Max. Throughput (Mbps)		54	54	54	54
Total Load (Mbps)		30	45	54	60
Load Ratio		0.556	0.833	1.000	1.111

B. Simulation Result s

Table 4 and Table 5 show the simulation results.

TABLE 4 SIMULATION RESULT OF 802.11b

802.11b		Case 1	Case 2	Case 3	Case 4
Load Ratio		0.545	0.818	0.982	1.364
Standard CW Method					
Achieved Throughput per group (Mbps)	Group 1	1.97	2.82	2.72	2.71
	Group 2	3.70	2.96	2.76	2.75
Total Achieved Throughput (Mbps)		5.67	5.78	5.47	5.47
Achievement Ratio	Group 1	0.99	0.94	0.75	0.54
	Group 2	0.93	0.49	0.38	0.28
Jain's Fairness Index		0.9982	0.9109	0.9033	0.9034
Total Collisions		5,194	3,908	8,496	8,640
Total Successful Transmissions		42,536	43,326	41,058	40,999
Proposed CW Method					
Achieved Throughput per group (Mbps)	Group 1	1.99	2.29	2.53	2.07
	Group 2	3.90	3.66	3.28	3.95
Total Achieved Throughput (Mbps)		5.89	5.95	5.80	5.80
Achievement Ratio	Group 1	0.99	0.76	0.70	0.51
	Group 2	0.97	0.61	0.45	0.33
Jain's Fairness Index		0.9995	0.9842	0.9538	0.9974
Total Collisions		1,210	1,200	3,135	3,101
Total Successful Transmissions		44,162	44,639	43,508	45,175

TABLE 5. SIMULATION RESULT OF 802.11a

802.11a		Case 1	Case 2	Case 3	Case 4
Load Ratio		0.556	0.833	1.000	1.111
Standard CW Method					
Achieved Throughput per group (Mbps)	Group 1	10.02	13.96	14.01	14.04
	Group 2	17.47	14.00	13.91	13.87
Total Achieved Throughput (Mbps)		27.48	27.96	27.92	27.91
Achievement Ratio	Group 1	1.00	0.93	0.78	0.70
	Group 2	0.87	0.47	0.39	0.35
Jain's Fairness Index		0.9952	0.9006	0.8982	0.8969
Total Collisions		33,340	30,904	31,208	31,274
Total Successful Transmissions		206,136	209,676	209,380	209,322
Proposed CW Method					
Achieved Throughput per group (Mbps)	Group 1	10.00	14.02	14.12	13.85
	Group 2	19.99	17.66	17.57	17.82
Total Achieved Throughput (Mbps)		29.99	31.68	31.69	31.67
Achievement Ratio	Group 1	1.00	0.93	0.78	0.69
	Group 2	1.00	0.59	0.49	0.45
Jain's Fairness Index		0.9999	0.9503	0.9479	0.9542
Total Collisions		6,414	5,567	5,462	5,632
Total Successful Transmissions		224,958	237,576	237,676	237,528

The maximum achieved throughput of the entire network is about 6Mbps for 802.11b and 32Mbps for 11a after saturation or where Load Ratio is 1.0 and higher. These are considered to be reasonable with taking overhead such as DIFS, SIFS, ACK and back-off time into account. The proposed method shows definitely better throughput than the standard method. As it can be seen in the tables, the number of collisions is smaller with the proposed method. Generally, the sum of successful transmissions and collisions are similar between the proposed and standard methods. With the proposed method, a substantial amount of collisions are converted to successful transmissions.

Fig. 1 and Fig. 2 show the graphs of Load Ratio versus Achievement Ratio. In the graph, STD, PRP mean Standard CW Method, Proposed CW Method, and GP means node Group, respectively. Achievement Ratio is the ratio of Achieved Throughput to Required Throughput per Group.

If fairness of throughput is completely achieved, Achievement Ratio of Group 1 and 2 should become the same value. But Group 1 shows higher Achievement Ratio than Group 2 in Fig.1 and 2. This is because Group 1 has a lower required throughput and the required transmission air

 ISBN: 978-1-61208-454-1

time is shorter. In a saturated network, each node competes to secure its air time. The standard method provides a homogeneous opportunity to access the channel to all nodes. Therefore this is understandable that Group 1 can have higher Achievement Ratio as Group 1 needs totally shorter air time. The proposed method adjusts the CW based on the achieved and required throughput, but, still, CW has its limitation (i.e., CWmax as 1023). So the proposed method is considered to have better fairness than the standard method, but its fairness still has certain limitation.

In order to evaluate fairness, Jain's Fairness Index [11] is selected. Fig. 3 and Fig. 4 show the graphs of Jain's Index for 802.11b and 11a, respectively. As it can be seen in Fig. 3 and 4, Jain's Fairness Index is always higher with the proposed method.

IV. CONCLUSION

In this paper, we have proposed a new QoS control method for the ad hoc W-LAN network based on the DCF which handles the communication priority in accordance with each node's required and achieved bit rate. The computer simulation shows that the proposed method has better total throughput, fairness and collision numbers. The total throughput and Jain's Fairness Index are improved by several percentages. The number of collisions is one order of magnitude smaller and the number of successful transmissions was increased by a similar number.

This time, the proposed method has the maximum limit of CW, 1023, and this limitation may cap the effect. An infinite size for the CW is not practical, but we need to find an optimized maximum CW for the proposed method. This will be the subject of future work.

REFERENCES

[1] N. H. Vaidya, P. Bahl, and S. Gupta, "Distributed Fair Scheduling in a Wireless LAN," Proc. Of ACM MOBICOM2000, pp. 167-178, Boston, MA USA, Aug. 2000

[2] S. Park, K. Kim, D. C. Kim, S. Choi, and S. Hong, "Collaborative QoS Architecture between Diffserv and 802.11e Wireless LAN," Proc. Of IEEE VTC'03-Spring, Jeju, Korea, April 2003

[3] S. Choi, J. D. Prado, S. S. Ni, and S. Mangold, "IEEE 802.11e contention-based channel access (EDCF) performance evaluation," Proc. ICC2003, pp. 1151-1156, Anchorage, Alaska, USA, May 2003

[4] X. Yu, P. Navaratnam and K. Moessner, "Resource Reservation Schemes for IEEE 802.11-Based Wireless Networks: A Survey," IEEE COMMUNICATIONS SURVEYS & TUTORIALS, vol. 15, no. 3, pp. 1042 - 1061, Nov. 2012.

[5] M. Heusse, F. Rousseau and A. Duda, "Idle Sense: An Optimal Access Method for High Throughput and Fairness in Rate Diverse Wireless LANs," Porc. ACM SIGCOMM'05 vol. 35, no. 4, 2005

[6] Y. He, J. Sun, R. Yuan and W. Gong, "A Reservation Based Backoff Method for Vide Streaming in 802.11 Home Networks," IEEE J. Sel. Commun., vol. 28, no. 3, 2010.

[7] Q. Zhang and Y. Zhang, " Cross-Layer Design for QoS Support in Multihop Wireless Network," Proceedings of IEEE, Vol.96, No.1, pp. 64 – 79, Jan. 2008.

[8] L. Romdhani, Q. Ni and T. Turletti, "Adaptive EDCF : Enhanced Service Differentiation for IEEE 802.11 Wireless Ad-Hoc Networks", IEEE Wireless Communications and Networking Confernce 2003 (WCNC2003), pp. 23-27, March 2003.

[9] J. Maeda, R. Shinkuma and T. Takahashi, "QoS Control Method of DCF Wireless LAN for Supporting Required Bit Rate", Technical Repoer of IEICE NS 2004-3, pp. 52-56, April 2004.

[10] A. Matoba, T. Sasagawa, M. Hanada and M. W. Kim, "QoS Management Method for W-LAN Network Considering Hidden Node Issue", World Congress on Computer and Information Technology 2013 (WCCIT 2013), pp. 101-105, June 2013.

[11] R. Jain, A. Durresi and G. Babic, "Throughput Fairness Index: An Explaination," The Ohio State University, Columbus, OH 43210, 1999.

 ISBN: 978-1-61208-454-1

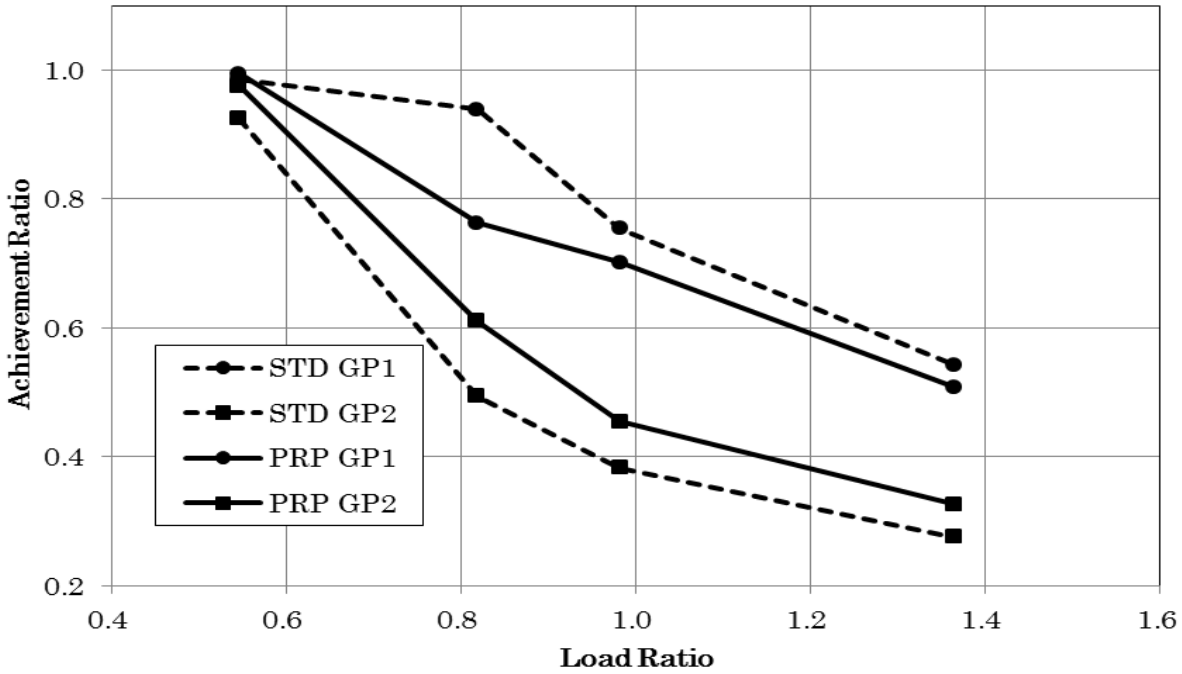

Figure 1. Achievement Ratio of 802.11b

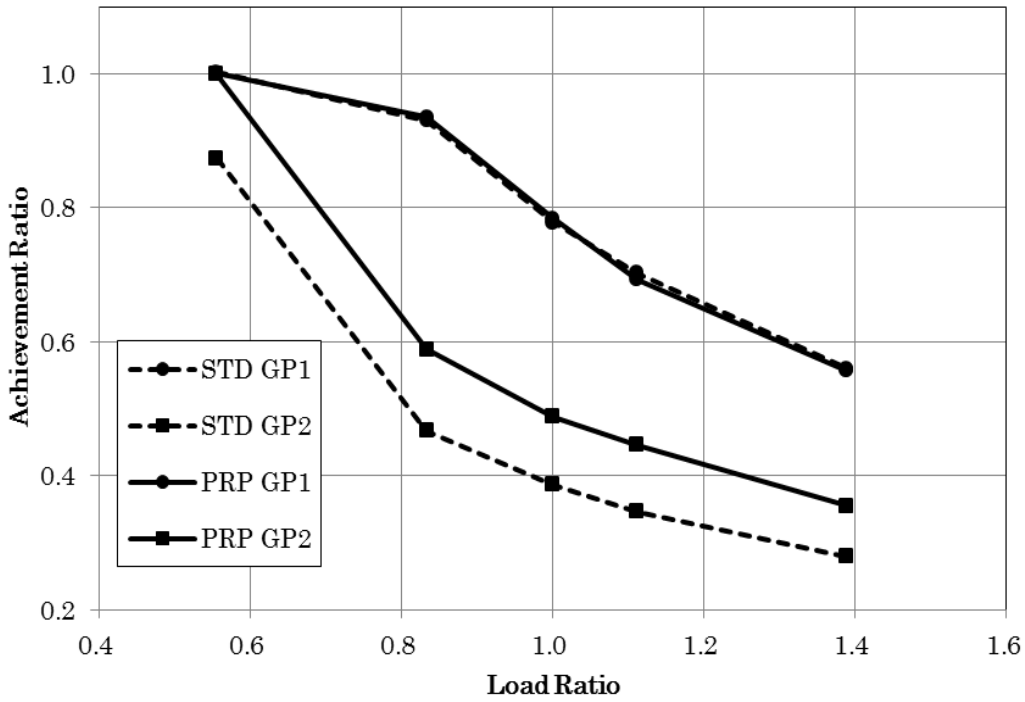

Figure 2. Achievement Ratio of 802.11a

 ISBN: 978-1-61208-454-1

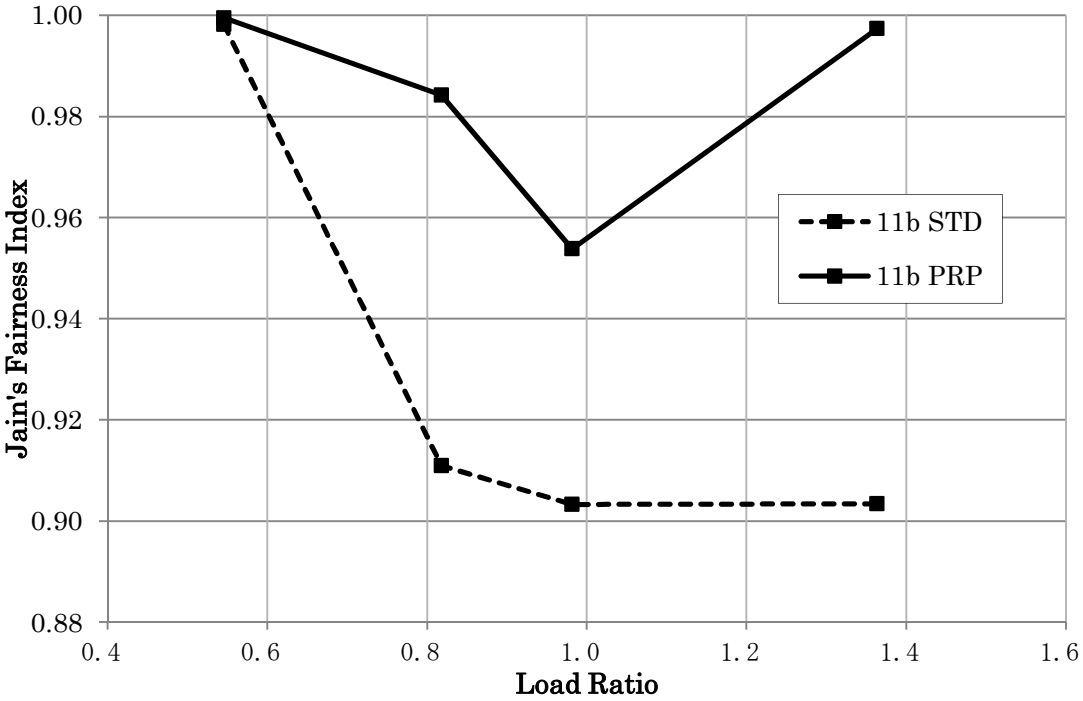

Figure 3. Jain's Fairness Index of 802.11b

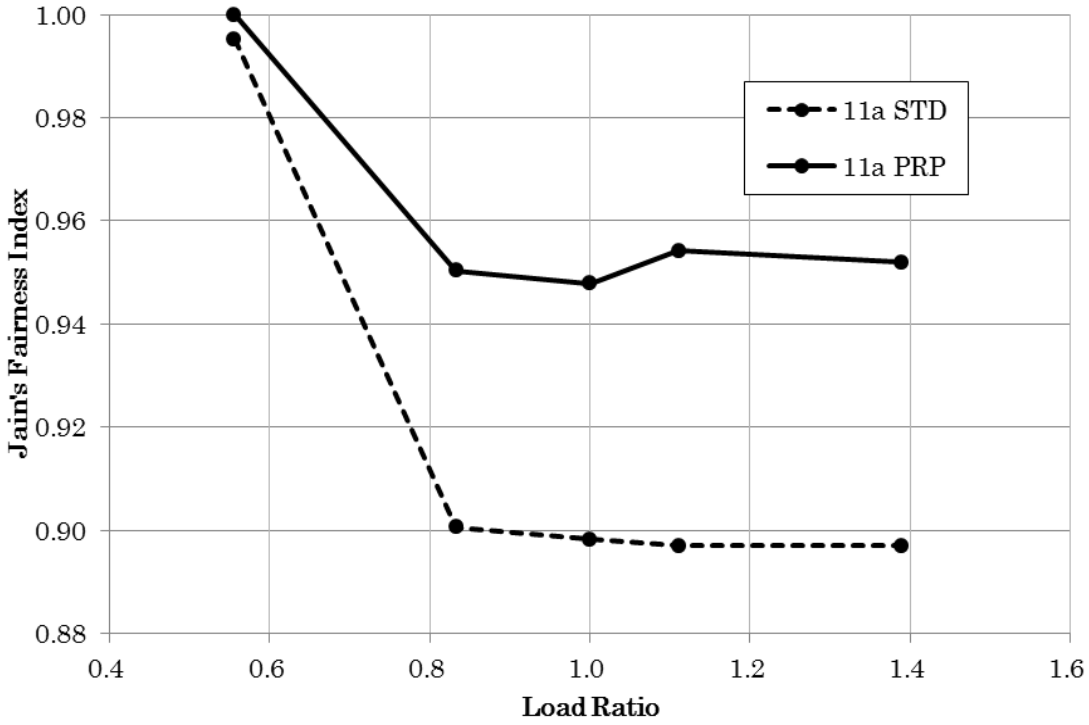

Figure 4. Jain's Fairness Index of 802.11a

 ISBN: 978-1-61208-454-1

Enhanced Indoor Positioning Method based on IEEE 802.11 RSSI Considering DOP in Building Environments

Jun Gyu Hwang, Giovanni Escudero, Jingjing Wang, Joon-Goo Park
School of Electronics Engineering
Kyungpook National University
Daegu, Republic of Korea
email: cjstk891015@naver.com, gioescudero@gmail.com, wjj0219@naver.com, jgpark@knu.ac.kr

Kwang Eog Lee
Agency for Defense Development
Daejeon, Republic of Korea
email: kelee@add.re

***Abstract*—The demand for Location Based Service (LBS) is increasing in the development of communication and mobile technologies. Moreover, location determination technologies especially for indoor environments are getting a lot of attention. Most indoor positioning methods just make use of Received Signal Strength Indicator (RSSI) measurements that generate from the same floor. However, usually RSSI measurements are available from different floors. In that case, we have to consider the Dilution of Precision (DOP) used in satellite positioning systems. With this in mind, we can choose a better Access Point (AP) configuration than that of when using only APs in the same floor. In this paper, to improve the accuracy of indoor positioning, we propose an indoor positioning method that includes APs placed in different floors and takes into consideration the DOP.**

Keywords-LBS; DOP; RSSI; Indoor Positioning; Wi-Fi.

I. INTRODUCTION

Positioning technologies can be separated into two groups, that is, outdoor positioning and indoor positioning. In outdoor positioning, Global Positioning System (GPS) [1] is a common example of such technologies. In indoor positioning, several methods, WLAN, Bluetooth, ZigBee, etc., have been developed depending on the situation [2]. However, WLAN measurement based indoor positioning methods are becoming a strong candidate for positioning in such environments.

The existing methods for indoor positioning that we evaluate, usually, take advantage of the properties that the received signal strength has, to determine the distance from an AP to a mobile station, in order to obtain its location [3].

Usually, indoor positioning methods based on IEEE 802.11 WLAN information only make use of RSSI measurements that generate from the same floor. However, in regular indoor environments such as commercial or office buildings, RSSI measurements from APs in different floors can be detected, and dilution of precision can be used to increase the accuracy of these measurements [4].

Given this, in the following paper, we propose an indoor positioning method that considers APs in different floors in order to increase the accuracy of the positioning system.

This paper presents in its second section descriptions for the RSSI penetrated channel model and for dilution of precision. The third section introduces the proposed positioning method using DOP and an overview of the simulation parameters and results. In section four, we present our conclusions.

II. RSSI PENETRATED CHANNEL MODEL AND DOP

A. RSSI Penetrated Channel Model

The RSSI defines a measurement of the RF energy and its unit is dBm. The RSSI decreases exponentially as the distance from the AP increases. Because of these characteristics, in this paper we use an RSSI attenuation model given by [5]

$$\mathrm{RSSI[dBm]} = -10n \log_{10} \frac{d}{d_0} + A \quad (1)$$

$$\mathrm{d[m]} = 10^{\frac{\mathrm{RSSI}-A}{-10n}}. \quad (2)$$

In (1), n is the attenuation factor, parameter A is the offset which is the measured RSSI value at a reference point (usually 1 meter) from the AP. And d is the distance from the AP to the point of measurement. d_0 is the reference point distance. These parameters reflect the indoor propagation environment. Because RSSI is a sensitive parameter, it is affected by the environment significantly.

In practical situations, many factors that can affect the RSSI value exist, such as furniture, walls, and people. These factors can produce signal scattering and multi-path effects. They can also result in positioning errors. In order to reduce positioning errors, proper parameter determination is necessary.

The penetrated channel model shows the RSSI when measured through an additional layer. Figure 1 shows a schematic of the penetrated channel model.

 ISBN: 978-1-61208-454-1

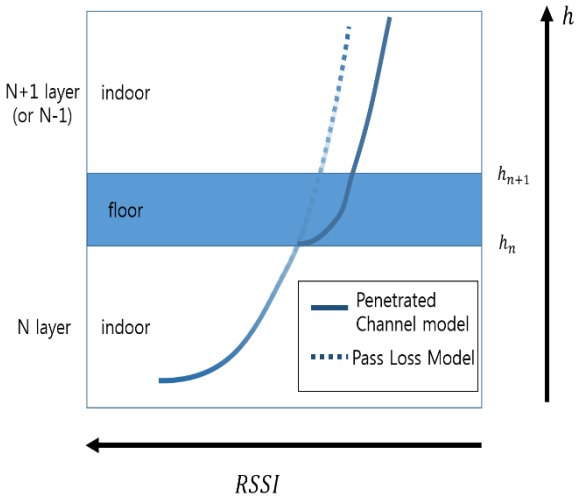

Figure 1. Penetrated Channel Model.

Each layer is separated by the floor. The floor has an attenuation factor which is different from the indoor environment. Also, the reference point changes from d_0 to h_n. Therefore the penetrated channel model equation in the floor is as follows:

$$\text{RSSI[dBm]} = -10n_f \log_{10}\frac{d}{h_n} + (-10n\log_{10} h_n + A). \quad (3)$$

In (3), n_f is the attenuation factor in the floor, height h_n is the distance between the floor layer and the ceiling layer. When an RF signal passes through the floor the attenuation factor comes back to n and the reference point changes to h_{n+1} which is the distance between one floor layer and the next. So, the penetrated channel model equation in the next layer is

$$\text{RSSI[dBm]} = -10n\log_{10}\frac{d}{h_{n+1}}h_n + \left(-10n_f\log_{10}\frac{h_{n+1}}{h_n} - 10n\log_{10} h_n + A\right). \quad (4)$$

By defining the penetrated channel model, even APs that are located on a different layer are available for positioning.

B. DOP(Dilution of Precision)

The effect of satellite geometry is quantified in the measure called Dilution of Precision, or DOP. DOP does not depend on anything that cannot be predicted in advance. It only depends on the positions of the GPS satellites relative to the GPS location of the receiver. The satellite position is known in advance, and GPS position is also fixed, thus the DOP of a GPS system can be calculated even without using the GPS system.

The problem of defining if the DOP is poor or good due to satellite geometry remains. When satellites are located at wide angles relative to each other, this configuration minimizes the error in position calculations. On the other hand, when satellites are grouped together or located in a line the geometry will be poor.

DOP is often divided into several components which are listed below [6]:

- VDOP: Vertical DOP
- HDOP: Horizontal DOP
- PDOP: Positional DOP
- GDOP: Geometric DOP

These components are used due to the variation of accuracy of the GPS system. The PDOP is most used among other components. The positioning error of PDOP is calculated from the data of GPS receiver multiplied by range error which is given by

$$\text{Positioning Error} = \text{Range Error} * \text{PDOP}. \quad (5)$$

A DOP of 2 means that whatever the range error was, the final positioning error will be twice as big.

For example, if the User Estimated Range Error (UERE) is 10 meters and the PDOP is 2, the final positioning error will be 20 meters.

1) Computation of DOP: As a first step of computing DOP, consider the unit vectors from the receiver to satellite *i* [6]

$$\left(\frac{x_i-x}{R_i}, \frac{y_i-y}{R_i}, \frac{z_i-z}{R_i}\right) \quad (6)$$

Where:

$$R_i = \sqrt{(x_i-x)^2 + (y_i-y)^2 + (z_i-z)^2}$$

x, y, z: position of the receiver

x_i, y_i, z_i: position of the satellite

The formula (6) in matrix form is given by

$$A = \begin{bmatrix} \frac{x_1-x}{R_1} & \frac{y_1-y}{R_1} & \frac{z_1-z}{R_1} & -1 \\ \frac{x_2-x}{R_2} & \frac{y_2-y}{R_2} & \frac{z_2-z}{R_2} & -1 \\ \frac{x_3-x}{R_3} & \frac{y_3-y}{R_3} & \frac{z_3-z}{R_3} & -1 \\ \frac{x_4-x}{R_4} & \frac{y_4-y}{R_4} & \frac{z_4-z}{R_4} & -1 \end{bmatrix} \quad (7)$$

The first three elements of each row of A are the components of a unit vector from the receiver to the indicated satellite. Since the number of APs is three, the minimum number of APs required, we assume the fourth vector to have an infinite value and thus set every element to -1.

Formulate the matrix, Q, as

$$Q = (A^T A)^{-1} = \begin{bmatrix} \sigma_x^2 & \sigma_{xy} & \sigma_{xz} & \sigma_{xt} \\ \sigma_{xy} & \sigma_y^2 & \sigma_{yz} & \sigma_{yt} \\ \sigma_{xz} & \sigma_{yz} & \sigma_z^2 & \sigma_{zt} \\ \sigma_{xt} & \sigma_{yt} & \sigma_{zt} & \sigma_t^2 \end{bmatrix} \quad (8)$$

From Q, the DOP can be calculated as

$$PDOP = \sqrt{\sigma_x^2 + \sigma_y^2 + \sigma_z^2} \quad (9)$$

 ISBN: 978-1-61208-454-1

III. PROPOSED POSITIONING METHOD AND SIMULATION

A. Proposed Positioning Method

We propose a method that is divided into two steps. First, we scan APs. Then, we measure the received signal strength indicator and determine on which floor the AP is located.

Next, we compute the DOP of each combination of APs. Then, a combination of three of the APs with the best DOP is selected and we use this combination for positioning.

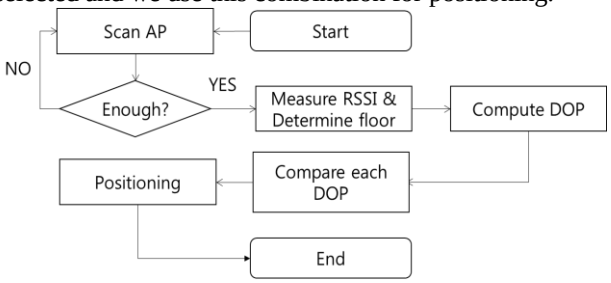

Figure 2. Proposed Positioning Algorithm

Figure 2 is a representation of the proposed positioning algorithm used in our method.

B. Simulation

We conducted experiments in Kyungpook National University's IT-1 building. This building's h_n is 2.57m, h_{n+1} is 3.74m, and the attenuation factor n is 2.9, n_f is 7.02.

We used IpTIME N3004 model APs, Broadcom laptop embedded wireless network cards, and software for collecting the RSSI.

Figure 3 shows the Cumulative Distribution Function (CDF) for both the existing method and the proposed method. Ninety percent of the proposed method's CDF is less than 1.2m. However, ninety percent of the existing method's CDF is less than 2.2m.

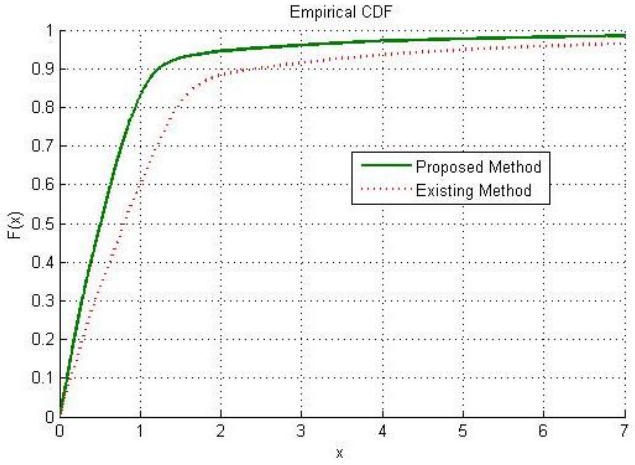

Figure 3. Proposed positioning algorithm results

TABLE I. SIMULATION RESULT

	Existing Method	Proposed Method
Average Error	1.56 m	1.24 m

As shown in Table 1, the positioning error of the proposed method is less than that of the existing method by 0.32 meters. The existing method uses an RSSI attenuation model in a WLAN environment without taking the DOP into consideration.

IV. CONCLUSIONS

This paper proposes an indoor positioning method using IEEE 802.11 WLAN RSSI measurements considering the penetrated channel model. In order to enhance indoor positioning accuracy, we use different layer APs. The proposed method in this paper can enhance the positioning accuracy in multilayer-buildings and wall-through indoor environments. The simulation results show that the positioning error of the proposed method is less than that of existing method by 0.32m.

In the future, an integrated model is necessary to consider penetration as well as diffraction. Also, when a positioning error occurs there is RSSI error as well. Given this, a filter for correcting the RSSI error should be developed.

V. ACKNOWLEDGMENTS

This work has been supported by the National GNSS Research Center program of Defense Acquisition Program Administration and Agency for Defense Development.

VI. REFERENCES

[1] M. Wright, D. Stallings, and D. Dunn, "The effectiveness of global positioning system electronic navigation", Southeast Con, 2003. Proceedings. IEEE, April 2003, pp. 4-6.

[2] H. Liu, H. Darabi, P. Banerjee, and J. Liu, "Survey of wireless indoor positioning techniques and systems" Systems, Man, and Cybernetics, Part C: Applications and Reviews, IEEE Transactions on 37.6 (2007), November 2007, pp. 1067-1080.

[3] S. Mazuelas et al., "Robust Indoor Positioning Provided by Real-Time RSSI Values in Unmodified WLAN Networks", Selected Topics in Signal Processing, IEEE Journal of (Volume: 3, Issue: 5), October 2009, pp. 821-831.

[4] S. Zirari, P, Canalda, and F. Spies, "Geometric and Signal Strength Dilution of Precision (DoP) Wi-Fi", IJCSI International Journal of Computer Science Issues, Vol. 3, 2009, pp. 35-44.

[5] S. Park, D. Park, A. S. Kim, J. Park, S. Kim, and J. G. Park, "A study on enhanced indoor localization method through IEEE 802.11 signal strength measurement" KSII The first International Conference on Internet (ICONI) 2009, December 2009, pp. 761-764.

[6] R. B. Langley, "Dilution of precision", GPS World, May 1999, pp. 52-59.

 ISBN: 978-1-61208-454-1

A Novel Tap Selection Design for Filters in Unequal-Passbands Scheme

Salah Al-Din Badran
Sohar University
P. Code 311
Sohar, Oman
email: sbadran@soharuni.edu.om

Samad Ahmadi, Pooneh Bagherizadeh
CSI School, DMU University
Leicester, uk
email: sahmadi@dmu.as.uk;
pooneh.bagherizadeh@dmu.ac.uk

Ismail Shahin
Department of Engineering
University of Sharja
Sharja, UAE
email: ismail@sharjah.ac.ae

***Abstract*—A filter bank divides the input signal into *L* bands having different passbands called unequal-passbands-filter bank. This type of filter bank can be obtained in various ways, for example, from an equal-passbands-bank in which the signals of each band are combined to produce new unequal-passbands. Recent results showed that the unequal-passbands scheme has superior performance over the equal-passbands scheme. In this paper, a new method showing a decrease in the number of taps in the separation stage of the blind source separation system is presented. Decreasing number of taps is necessary to decrease the complexity cost. The simulation results prove that the proposed technique improves the convergence using filter bank in octaves with decomposition which was observed for colored input that has low-pass characteristics.**

Keywords- Filter bank; multiband; convergence; adaptive filters; taps.

I. INTRODUCTION

In recent years, some schemes for adaptive filtering were presented with the aim to accelerate the convergence to input signals correlated over time (color signals). In some cases, the aim was to reduce the computational cost, promoting the coefficients of the adaptive filters whose sampling rate is below that of the input signal. However, these schemes have an input-output delay and spectrum overlap between the various bands that should be reduced in advance promote adaptation of the filters [1]. Marelli and Minyue [2] proposed a scheme with maximum decimation able to make almost an exact modeling of the Finite Impulse Response (FIR) systems, through the insertion of cross filters and considering that there is spectrum overlapping between adjacent bands. In this case, both the input signal and the desired signal was decomposed into multiple bands, and the error generated in each band was used to update the respective adaptive filters (direct and crossed) related to the band.

Papoulis and Stathaki [3] proposed two schemes of non-maximally decimated ($F < L$) filter banks. As the effect of the overlapping spectrum is directly proportional to the decimation factor, the lower the value of F the smaller the minimum mean square error of the scheme. For fixed values of L and F, one can obtain optimum filter bank that minimizes the mean square error of the final scheme. The difference between the two proposed schemes is that the desired signal is decomposed into multiple bands, while the other one the final error of the scheme is decomposed.

Two other schemes have been proposed by Lian and Wei [4] and Brown [5]. Papoulis and Stathaki [3] use analysis bank without decimation, followed by adaptive filters of nonzero coefficients, whereas Brown's algorithm [4], which was derived from the first, uses a maximally decimated filter bank with perfect reconstruction and adaptive filters operate at reduced rate.

New research presented by McCloud and Etter [6], and Kim and Choi [7], showed that the error in the scheme is decreased in adaptive filters with *unequal-passbands* in analogy to the *equal-passbands*. The *unequal-passbands*-schemes presented in [6] employ noncritical decimation of the multi-band signals. In this work an *unequal-passbands*-scheme with maximally decimated random bands is proposed. The contribution of this paper is derivation of the unequal-passbands maximally decimated scheme from unequal-passbands scheme without decimation, which employs analysis bank and filters with nonzero-coefficients that are used to construct an equivalent FIR system. The rest of the paper is organized as follows: adaptive filter scheme without decimation is discussed in Section II, maximally decimated scheme with unequal-passbands and the extraction of the total number of taps used in the proposed scheme is presented in Section III, simulation results is discussed in Section IV and finally, the paper is concluded in Section V.

II. ADAPTIVE SCHEMES WITHOUT DECIMATION

The adaptive scheme is shown in Figure 1 and uses filters with nonzero coefficients that are capable of modeling only a particular class of FIR systems and cannot be generalized for all FIR systems because the length of analysis filters is greater than the number of adaptive coefficients. However, Apolibario and Alves [8] show that by a suitable selection of the filter, better parameters can be obtained to model the FIR system. We propose in Figure 1 a scheme that can model any FIR system but will include some delay.

 ISBN: 978-1-61208-454-1

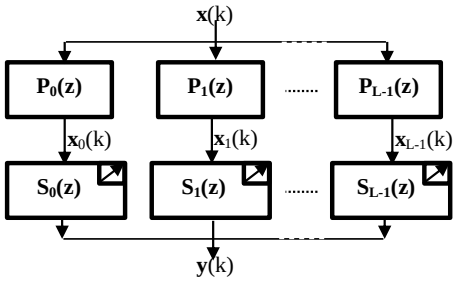

Figure 1. Scheme explains the use of adaptive filters.

Considering the analysis polyphase bank representation of the scheme in Figure 1, the polyphase matrix of dimension $L \times L$ is defined as [9]:

$$\mathbf{P}_m(z) = \begin{bmatrix} P_{0,0}(z) & P_{0,1}(z) & \cdots & P_{0,L-1}(z) \\ P_{1,0}(z) & P_{1,1}(z) & \cdots & P_{1,L-1}(z) \\ \vdots & \vdots & \ddots & \vdots \\ P_{L-1,0}(z) & P_{L-1,1}(z) & \cdots & P_{L-1,L-1}(z) \end{bmatrix} \quad (1)$$

where $P_{r,c}(z)$ are polyphase components of the r^{th} analysis filter $P_r(z) = \sum_{k=0}^{K_p-1} P_r(k) z^{-k}$, given by

$$P_{r,c}(z) = p_r(c) \sum_{k=1}^{K_p-1} p_r(kL + c) z^{-k} \quad (2)$$

where K_p is the length of the analysis filters.

Therefore, the system function used in Figure 1 can be expressed as:

$$P(z) = [S_0(z) S_1(z) \cdots S_{L-1}(z)] \mathbf{P}_m(z) \left(\begin{bmatrix} 1 & z & \cdots & z^{L-1} \end{bmatrix}^T \right)^{-1}. \quad (3)$$

The taps of the filters of nonzero coefficients $S_r(z)$ are changed to give us the equivalent FIR scheme, which will be called $U(z)$. The decomposition of the polyphase transfer function of the unknown system is given by

$$U(z) = [U_0(z) U_1(z) \cdots U_{L-1}(z)] \left(\begin{bmatrix} 1 & z & \cdots & z^{L-1} \end{bmatrix}^T \right)^{-1}. \quad (4)$$

From Equations (3) and (4), it can be seen that the scheme accurately models an unknown FIR system when

$$[S_0(z) S_1(z) \cdots S_{L-1}(z)] \mathbf{P}_m(z) = [U_0(z) U_1(z) \cdots U_{L-1}(z)]. \quad (5)$$

Equation (5) shows that the equality cannot be achieved as the length of the adaptive filters of nonzero coefficients is $L\kappa$ and the length of the analysis filters is K_p, while the product $S_r(z)P_r(z)$ has length $K_p + L_k - 1$, which is greater than the number of coefficients $L\kappa$ that was adapted. However, if

$$[S_0(z) S_1(z) \cdots S_{L-1}(z)] = [U_0(z) U_1(z) \cdots U_{L-1}(z)] \mathbf{Q}_m(z) \quad (6)$$

such that $\mathbf{Q}_m(z)\mathbf{P}_m(z) = \mathbf{I}$, where $\mathbf{I}$ is the unit matrix of dimension $L \times L$ with delay, the system function in Figure 1 will be

$$P(z) = U(z). \quad (7)$$

but with delayed $U(z)$. The matrices $\mathbf{P}_m(z)$ and $\mathbf{Q}_m(z)$ that satisfy the above conditions are, respectively, the polyphase matrix of the analysis and synthesis filter bank with perfect reconstruction. The synthesis polyphase bank matrix is defined as

$$\mathbf{Q}_m(z) = \begin{bmatrix} Q_{0,0}(z) & Q_{1,0}(z) & \cdots & Q_{L-1,0}(z) \\ Q_{0,1}(z) & Q_{1,1}(z) & \cdots & Q_{L-1,1}(z) \\ \vdots & \vdots & \ddots & \vdots \\ Q_{0,L-1}(z) & Q_{1,L-1}(z) & \cdots & Q_{L-1,L-1}(z) \end{bmatrix} \quad (8)$$

where $Q_{r,c}(z)$ are polyphase components of the r^{th} synthesis filter $Q_r(z) = \sum_{k=0}^{K_q-1} q_r(k) z^{-k}$ is given by

$$\mathbf{Q}_{r,c}(z) = q_r(L - (c+1)) \sum_{k=1}^{K_q-1} q_r(kL - c + L - 1) z^{-k} \quad (9)$$

where K_q is the length of the synthesis filters.

Then, using an analysis filter bank, which allows perfect reconstruction and adaptive filters of nonzero coefficients with sufficient order to satisfy (6), the scheme of Figure 1, now can implement exactly the FIR system with transfer function given in equation (7). However, it should be emphasized that the delay introduced by the filter bank needs to be considered in the adaptation algorithm of the filters coefficients.

For lengths K_{un} and K_{pr} of the unknown prototype systems, respectively, the number of nonzero coefficients K must be at least:

$$\kappa = K_{un} + K_{pr} - 1. \quad (10)$$

 ISBN: 978-1-61208-454-1

III. MAXIMALLY DECIMATED SCHEME WITH UNEQUAL-PASSBANDS

An analysis filter bank of unequal-passbands can be configured from the adaptive scheme of unequal-passbands shown in Figure 1, but employs analysis filters bank with unequal-passbands. This scheme is shown in Figure 2. The input signal $x(k)$, and $P_i(z)$ indicates the analysis of unequal-passbands with L-bands, the adaptive filters of nonzero coefficients will be denoted as $S_i(z)$, the required signal will be $\mathfrak{d}(k)$, where the error signal is $e(k)$.

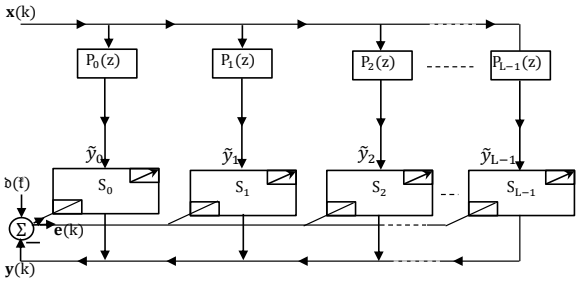

Figure 2. Adaptive Scheme of unequal-passbands without decimation.

The perfect reconstruction analysis filter bank of L-bands has orders

$$K_{P_0} = \sum_{c=0}^{L-1} 2^c K_{P^{0,c}}, \quad K_{P_i} = \sum_{c=0}^{L-i} 2^c K_{P^{0,c}} + 2^{L-i-1} K_{P^{1,c}} \tag{11}$$

Where $K_p^{0,c}$ are orders of $P^{0,c}(z)$ and $K_p^{1,c}$ are orders of $P^{1,c}(z)$.

The filters of unequal-passbands and with perfect reconstruction analysis $P_i(z)$ and synthesis filters $Q_i(z)$ are included after each of the sub-adaptive filter in Figure 2.

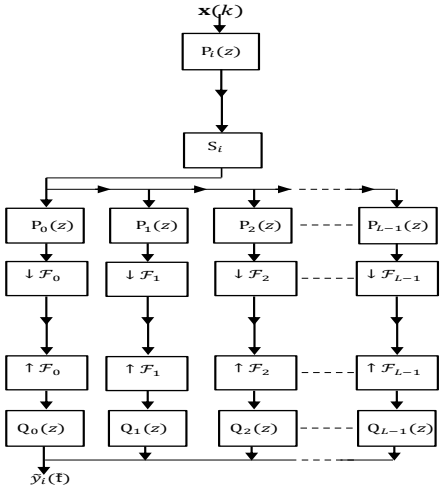

Figure 3. i^{th} band after implying the maximally sampled filter bank.

Figure 3 shows the i^{th} band of the resulting scheme, which allows the filters to operate at a lower sampling rate.

To obtain a scheme with less complexity we consider the analysis filters are sufficiently selective to accept spectrum interference only in frequency responses of neighboring bands. The i^{th} band that is shown in Figure 4, we see that $P_{r,c}(z) = P_r(z)P_c(z)$ are the filters of nonzero coefficients $S_i(z)$ shifted forward by F_i [10]. Looking at the i^{th} band of the simplified scheme shown in Figure 4, the sampling rate of the adaptive filters is F_i and F_{i+1} times less than the rate of the input signal.

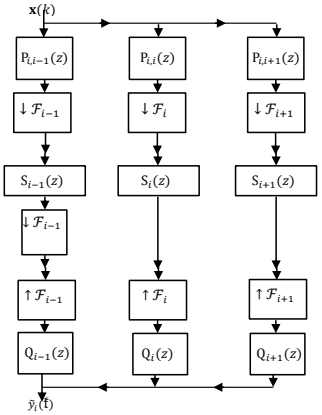

Figure 4. Adaptive filters work at lower rates.

The scheme can be further simplified by noting that $P_{r,c}(z) = P_{c,r}(z)$ and combining the signals in adjacent bands.

A. Taps Selection

As mentioned in section III, about a good design of analysis filters to avoid the spectrum overlap, the parameters of Figure 4 are similar to the parameters of Figure 2. From this hypothesis an equation will be extracted assuming the case of modeling a random FIR system.

The adaptive filters $S_i(z)$ of each band of Figure 2 are described by shifting $\chi_i = 1/F_i$ [11].

Defining $S_i(z)$ as follows:

$$\mathbf{S}_i(z) = \left[S_{i,0}(z) S_{i,1}(z) \cdots S_{i,\chi_{i-1}}(z)\right]^T \tag{12}$$

and $S(z)$ is constructed by L filters $S_i(z)$, given by

$$\tilde{\mathbf{S}}(z) = \left[\tilde{S}_0(z)\tilde{S}_1(z)\cdots\tilde{S}_{\chi_0-1}(z)\right]^T = \left[S_0^T(z)S_1^T(z)\cdots S_{L-1}^T(z)\right]^T. \tag{13}$$

$\mathbf{P}_m(z)$ is the matrix of dimension F_0 x F_0 contains analysis polyphase filters components - type I, given by

$$\mathbf{P_m}(z) = \left[\mathbf{P}_0^{\mathbf{T}}(z)\mathbf{P}_1^{\mathbf{T}}(z)\cdots\mathbf{P}_{L-1}^{\mathbf{T}}(z)\right]^T \tag{14}$$

where $\mathbf{P}_i(z)$ is the matrix $\chi_i \mathbf{x} F_i$ with the r^{th} row (r=0,. χ_i).

The system function applied for the scheme of unequal-passbands in Figure 2 can be expressed as:

$$\mathcal{T}(z) = \tilde{S}^T(z)\mathbf{P}_m(z)\begin{bmatrix}1 & z^{-1} & \cdots & z^{-\mathcal{T}_0}\end{bmatrix}^T \quad (15)$$

To identify the unknown system, taps of $S_i(z)$ can be adjusted to match the required FIR scheme. The system function of the unknown system is denoted by $U(z)$ and written as

$$U(z) = \begin{bmatrix}U_0(z) & U_1(z)\cdots U_{L_0-1}(z)\end{bmatrix}\begin{bmatrix}1 & z^{-1} & \cdots & z^{-\mathcal{T}_0}\end{bmatrix}^T \quad (16)$$

From equations (15) and (16), the multiband scheme accurately matches a FIR filter $U(z)$ at

$$U(z) = \begin{bmatrix}U_0(z) & U_1(z)\cdots U_{L_0-1}(z)\end{bmatrix}\begin{bmatrix}1 & z^{-1} & \cdots & z^{-\mathcal{T}_0}\end{bmatrix}^T. \quad (17)$$

and

$$\tilde{\mathbf{S}}^T(z)\mathbf{P}_m(z) = \begin{bmatrix}U_0(z) & U_1(z) & \cdots & U_{\mathcal{T}_0}(z)\end{bmatrix}. \quad (18)$$

Multiplying both sides of equation (18) by the matrix $Q_m(z)$:

$$\mathbf{P}_m(z)\mathbf{Q}_m(z) = \mathbf{I}, \quad (19)$$

where I is the unit matrix with delays, and its dimension is F_0 x F_0, and

$$\tilde{\mathbf{S}}^T(z) = \begin{bmatrix}U_0(z) & U_1(z) & \cdots & U_{\mathcal{T}_0}(z)\end{bmatrix}\mathbf{Q}_m(z) \quad (20)$$

with delays. The matrix $Q_m(z)$ satisfying (19) corresponds to the synthesis polyphase filters matrix which results in a system with perfect reconstruction [12].

The matrix $\mathbf{Q}_m(z)$ is of dimension F_0 x F_0 containing components of the expanded synthesis polyphase filters, given by

$$\mathbf{Q}_m(z) = \begin{bmatrix}\mathbf{Q}_0(z) & \mathbf{Q}_1(z) & \cdots & \mathbf{Q}_{L-1}(z)\end{bmatrix} \quad (21)$$

where $\mathbf{Q}_i(z)$ is an $F_0 \mathbf{x} \chi_i$ matrix with the r^{th} column (r = 0, $\cdots$, χ_i).

The parameters of the i^{th} S-band filter $\breve{S}_i(z)$, assuming the existence of overlapping spectrum only between adjacent bands, are given by

$$\breve{S}_i(z) = \sum_{r=0}^{\chi_i} z^{-r} S_{i,r}(z) \quad (22)$$

where filters $S_{i,r}(z)$ are related to $\breve{S}_i(z)$ through equations (12) and (13).

According to equations (20) and (22) for a scheme of unequal-passbands with L-band synthesis filters with $K_{Q_i}(z)$, we can write

$$K_{S_i} = K_U + K_{Q_i} \quad (23)$$

where K_{Si} is the minimum number of taps for the filters and K_U is the required system order.

Then, using a filter bank, which allows perfect reconstruction of unequal-passbands and adaptive filters of nonzero coefficients with sufficient orders that satisfies equation (23). However, it should be emphasized that the delay introduced by the filter bank should be considered in the adaptation algorithm.

IV. SIMULATION RESULTS

A random signal with normal distribution was applied on an IIR filter with z = 0.73. A noise of 10^{-7} is used and a system of order K_U = 900 is considered. The decomposition was in octaves with L = 1, 2, 3, 4. Table I shows the parameter of the unequal-passbands scheme the downsampling parameters F_i, and the orders of the analysis filters χ_i, respectively and L = 4 bands. Figure 5 shows the frequency responses of the corresponding analysis filters.

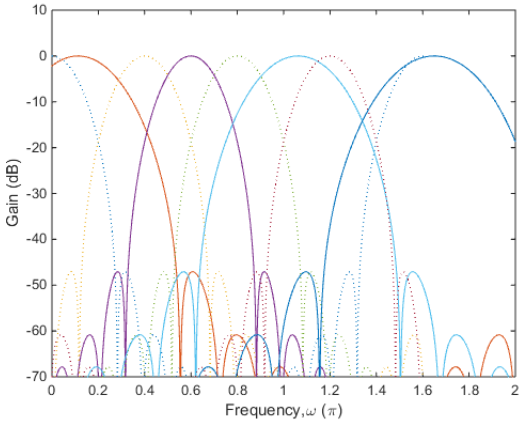

Figure 5. Frequency response of analysis filters

Figure 6 reflects the significant enhancement in the convergence rate of the proposed algorithm that can be obtained for colored input signals by increasing the number of bands in the multiband algorithm. In this research work, four bands for colored input were used that is enough to decorrelate their samples.

 ISBN: 978-1-61208-454-1

TABLE I. PARAMETERS OF THE UNEQUAL-PASSBANDS SCHEME

i	0	1	2
F_i	8	4	4
χ_i	1	2	2
K_{P_i}	332	332	155
K_{S_i}	149	149	256

Next, we compare the performance of mean square error considering different adaptive schemes with L = 4 bands. Figure 7 shows the performance of the mean square error for the proposed critical decimation scheme with unequal-passbands and the subsampled scheme with unequal-passbands. It can be seen that the suggested scheme with unequal-passbands offers faster convergence speed compared to the Ichikawa and Furukawa approach [13].

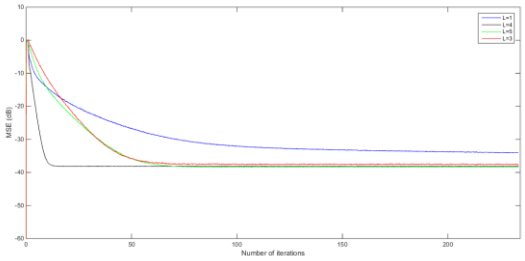

Figure 6. Performance of the mean square error of the scheme with unequal-passbands.

To decrease the problem of slow convergence in wider bands, we use a subsampled scheme.

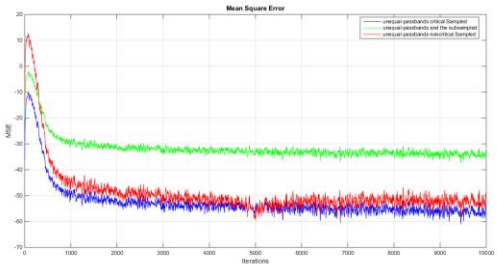

Figure 7. The mean square error with L = 4

The reason behind improving the convergence in the scheme with unequal-passbands in contrast to the one with equal-passbands is because of breaking down the input into narrower bands at the smaller frequencies that causes a lower rate between the largest and smallest powers [9].

V. CONCLUSION

In this paper, an unequal-passbands scheme was proposed and wider-band analysis filters were used. An equation is derived by modeling a random FIR system. This system is constructed from filters of nonzero coefficients that are used to design the equivalent FIR scheme. A perfect reconstruction is used by the help of the analysis filter bank. This bank allows us to obtain a scheme with less complexity by considering sufficiently selective analysis filters. By reducing the taps the computational cost is reduced. The results showed that the suggested method speeds up the convergence rate.

REFERENCES

[1] K. Kokkinakis and P. Loizou, "Subband-Based Blind Signal Processing for Source Separation in Convolutive Mixtures of Speech,"in IEEE International Conference on Acoustics, Speech and Signal Processing, ICASSP, Honolulu, 2007, pp. 917-920.

[2] D. Marelli and F. Minyue, "Performance analysis for subband identification,"IEEE Transactions on Signal Processing, vol. 52, no. 1, 2004, pp. 142 - 154.

[3] E. Papoulis and T. Stathaki, "Extension of generalised subband decomposition-based adaptive FIR structure," Electronics letters, vol. 39, no. 15, 2003, pp. 1157 - 1158.

[4] Y. Lian and L. Wei, "A computationally efficient nonuniform FIR digital filter bank,"Computers & Digital Techniques, IET, vol. 2, no. 4, 2009, pp. 285 - 294.

[5] J. Brown, "Generalized sampling and perfect reconstruction problem for maximally decimated filter banks," in International conference on Acoustics, Speech, and Signal Processing, 1989. ICASSP-89, Glasgow, 1989, pp. 577-580.

[6] M. Mccloud and D. Etter, "Subband adaptive filtering with time-varying nonuniform filter banks," in IEEE International Conference on Acoustics, Speech, and Signal Processing, Munich, 2010, pp. 1953-1956.

[7] S. Kim and Y. Choi, "A Subband Adaptive Filtering Algorithm Employing Dynamic Selection of Subband Filters," Signal Processing Letters, IEEE, vol. 17, no. 3, 2011, pp. 245 - 248.

[8] J. Apolinario and R. Alves, "Filtered gradient algorithms applied to a subband adaptive filter structure," in IEEE International Conference on Acoustics, Speech, and Signal Processing, Salt Lake City, UT, 2001, pp. 3705-3708.

[9] K. Lee and W. Gan, Subband Adaptive Filtering Theory and Implementation, 1st ed., West Sussex: John Wiley & Sons, 2009.

[10] M. Ljiljana, Multirate Filtering for Dogital Signal Processing: MATLAB Applications, New York: Information Science Reference, 2009.

[11] N. Fliege, Multirate Digital Signal Processing: MultirateSystems - Filter Banks - Wavelets, 1ST ed., Toronto: John Wiley & Sons, 1999.

[12] J. Gordana, Multirate Systems: Design and Applications: Design and Applications, 1st ed., London: Idea Group Publishing, 2000.

[13] Y. Ichikawa and T. Furukawa, "A new approach for non-uniform subband adaptive filtering," in IEEE International Symposium on Circuits and Systems, 2009, pp. 2271-2274.

 ISBN: 978-1-61208-454-1